

Reduction of Starting Current in Large Induction Motors

Mathew Habyarimana ¹, David George Dorrell ^{2,*}  and Remy Musumpuka ³

¹ Discipline of Electrical, Electronic and Computer Engineering, University of Kwazulu-Natal, Durban 4041, South Africa; hmatayoh@gmail.com

² School of Electrical and Information Engineering, University of the Witwatersrand, Johannesburg 4041, South Africa

³ R&D Division, Icarus Avionics (Pty), Durban 4075, South Africa; remmy.musumpuka@gmail.com

* Correspondence: david.dorrell@wits.ac.za; Tel.: +27-(0)11-7177244

Abstract: Large induction motors can have a high inrush and run-up current during starting, often up to ten times the rated current. In weak supplies, this could be a problem, causing system stability issues and the voltage to dip below acceptable levels. In islanded systems, the capacity could be pulled below its maximum. There are several different starting methods possible, but they are often only suitable for smaller machines. One method not investigated is the use of parallel capacitor compensation during the starting because large induction motors are very inductive during the starting sequence, so that supplying reactive power may be more effective than supplying energy. This paper first investigates several different induction motors with increasing size and assesses their compensation requirements in terms of the reactive power requirement during starting. It is shown that they do generally become more inductive as they increase in size. It is illustrated, using simulations, that using parallel capacitors during starting can significantly reduce the starting current. The concept is tested using a small experimental motor. Series inductors are added to the motor to make it more inductive and look more like a larger machine. The experimental results confirm that the method works. It is also found that the parallel capacitors require series filters to prevent harmonic current, and these can be realized using inductors in series with the compensation capacitors. Point-on switching using solid-state relays was tested, and these can reduce the transient switch-on current over the first voltage cycle.

Keywords: induction motors; starting; inrush current; power system



Citation: Habyarimana, M.; Dorrell, D.G.; Musumpuka, R. Reduction of Starting Current in Large Induction Motors. *Energies* **2022**, *15*, 3848. <https://doi.org/10.3390/en15103848>

Academic Editors: Jan Kiciński and Grzegorz Żywica

Received: 6 February 2022

Accepted: 25 March 2022

Published: 23 May 2022

Publisher's Note: MDPI stays neutral with regard to jurisdictional claims in published maps and institutional affiliations.



Copyright: © 2022 by the authors. Licensee MDPI, Basel, Switzerland. This article is an open access article distributed under the terms and conditions of the Creative Commons Attribution (CC BY) license (<https://creativecommons.org/licenses/by/4.0/>).

1. Introduction

Inrush currents when turning on a large load in a power system can cause problems. These are also called input surge currents or switch-on surges. They can result in excessive current being drawn. They can damage system equipment and cause destabilizing of weak grids. They can also cause protection relays to trip unnecessarily and cause voltages to dip and the malfunction of other connected apparatus.

Switch-on surges can be defined by the peak instantaneous electrical device current when first switched on [1,2]. Devices such as transformers, switch-mode power sources, and induction motors (IMs) all have large inrush currents. Large electromagnetic devices all have surges when switching on. These establish the magnetic field. IMs first have a magnetization surge, then a high run-up current if they are directly online connected. Five and ten times the rated full-load current can be drawn during the period when the machine is running up to speed.

If a large-load inrush current is not mitigated in some way, the supply busbar voltages can be pulled down and out of regulation. If the case is more serious, the system's current carrying capability can be exceeded. This could lead to overloading and a system trip.

Active power and reactive power are both drawn by IMs [3,4] since they are electromagnetic devices, possibly generating power quality issues if there is high inductive

loading. Capacitor compensation, which involves connecting parallel capacitors across a load, is often used in industry to improve poor plant power factors.

When starting a grid-connected IM, the slip is maximum ($s = 1$) at a standstill, and the induced rotor voltage is maximum—this is because of the frequency of the induced rotor voltage, called the slip frequency, is maximum. There is low rotor impedance, so there is a high rotor current. This is reflected in the stator by transformer action. As the speed increases, the slip frequency ($=sf_s$) decreases so that the induced rotor voltages, and hence rotor currents, decrease. At synchronous speed $s = 0$, there are no induced rotor voltages and currents. The large starting current is at a low power factor—and this becomes lower as the machine size increases, as discussed in this paper. The starting torque may be low depending on the size and design of the IM, especially in high-efficiency machines. In smaller machines, a high resistance or star-delta starter may be used to reduce the starting current, but in larger machines, this is usually not possible, as illustrated in this work. These starting methods reduce the starting current as well as the starting torque.

The use of capacitors in conjunction with induction motors is not new. They have been used for many decades in single-phase induction motors for both starting and running where they are in series with the auxiliary winding [5]. There have been studies of induction motors where they have been controlled electronically when in series [6,7] and in parallel to give a leading power factor correction and boost the output voltage during starting [8]. This could however have implications on the system with potential over-voltage as highlighted by [9]. None of these studies addressed the reactive power requirements of an IM. Power factor correction requirements were discussed by [10], though this was for steady-state operation.

This paper reports on a study that reduces the starting current in IMs using parallel capacitor compensation during IM starting. An inverter can be used in a smaller IM for starting current reduction where it becomes a variable speed drive (VSD). Unfortunately, in larger IMs, this is often too expensive. The costs involved in inverters were reviewed in [11] and are quite complex; however, when the inverter power increases beyond a few tens of kW, the cost will increase rapidly and not be linear with power ratings making their use very expensive when the power is into MW. While it is known that VSDs can lead to increased efficiency in many applications [12], for fan and pump motors, VSD operation is often not needed. During a large IM starting cycle, reactive power absorption is dominant, so it is possible to compensate for this using capacitors to generate reactive power. To mitigate the inrush current in an IM, this work develops models that are targeted at high-power IMs in remote grid locations or in islanded microgrids. If the motor is connected to a weak power system, the sudden high current can cause a temporary voltage drop, not only at the motor terminals, but the entire power bus feeding the starting motor [13]. Indeed, this problem is of a practical nature and was first highlighted in private discussions with an experienced electrical contractor who has had issues with large induction motors starting in major projects on several occasions—these were in applications such as water pumping stations and large air-conditioning fans and in motors that are at the end of a long feed line.

There is an analogy between IMs and transformers—their basic structure is two electrical circuits linked by a magnetic circuit. In terms of the equivalent circuit, the IM looks like a transformer but with the secondary windings shorted [14]. This is until the rotor starts to turn. This is when the rotor-circuit electro-mechanical energy conversion component (given by $(1 - s)/s \times R_2'$) becomes apparent. If there is a low mechanical load, then the starting transient is less; however, as with all rotating mechanical systems, there is inertia. Start-delta starting can be used in lower-power IMs. In this method, the 3-phase windings are connected in star to reduce the inrush current at the start, then reconnected in delta when running close to full load. High voltage machines are usually star-connected, which negates this method.

There are different methods for reducing inrush current in induction motors. These are:

- Star-delta starter [15];
- Autotransformer (reduced voltage);

- High resistance starter;
- Part Winding;
- Adjustable Frequency Drives (AFD) [16];
- Rotor resistance (wound rotor machine);
- DSTATCOMs [17];

In practice, apart from slip ring motors (which can be started by rotor resistance) and the AFD, the other methods reduce the starting torque as well as the inrush current. A method using an AFD and super-capacitors to give the energy for starting was reported in [16]. However, as discussed earlier, an AFD is an expensive solution in a large IM; with the other solutions really only suitable for smaller machines, there remains a need for an effective way to start larger IMs that reduces the starting current while maintaining starting torque.

Capacitor compensation will only address the reactive power demand, and studies have been done in the use of distribution static compensators (DSTATCOMs) in parallel with the motor during starting [17]. The system is shown in Figure 1. The disadvantages with this system are that it is expensive, and the DC capacitor on the DC side of the STATCOM needs to store most of the energy needed to start the machine to compensate for the motor power demand if it is controlled to compensate for energy drawn by the motor during starting and the reactive power. If it only compensates for the reactive power, then it is only doing the same as the parallel compensation capacitor method described here and will be more expensive due to the 3-phase inverter.

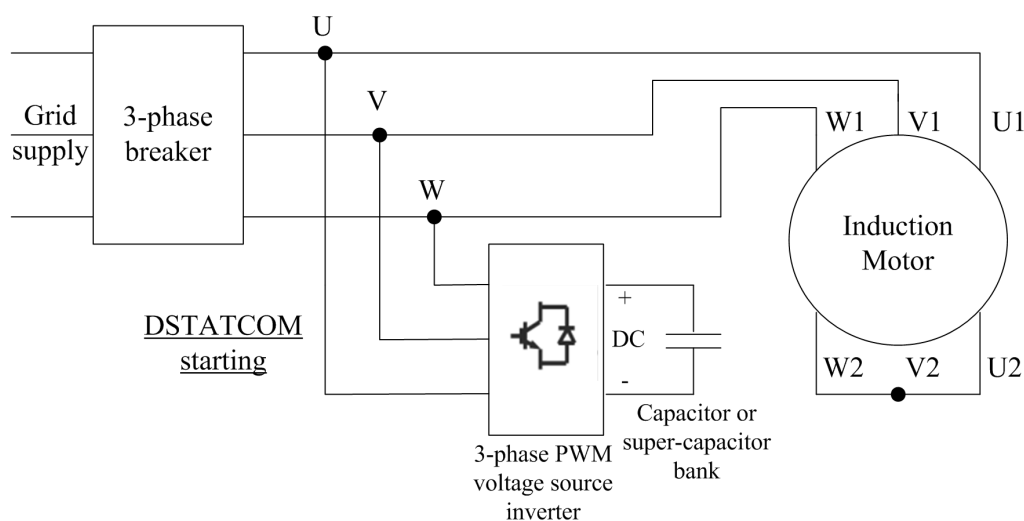


Figure 1. DSTATCOM induction motor starting.

Inrush current is associated with other significant effects on the supply and neighboring connections. These include:

- Supply voltage dips, where customers connected to the system experience the disturbance. This disturbance can contribute to the malfunction of sensitive electronics and can interrupt the supply to other equipment.
- The inrush current waveform is different from the normal AC sinusoidal and contains low and high frequency components. Such harmonics can interact with the filters installed in the system.
- The longer-period transient current offsets components of the inrush current, and can lead to oscillatory torque in motors resulting in increased motor vibration.

Devices such as AC electric motors, switched-mode power supplies (SMPS), incandescent lamps, power converters and transformers can draw several times their normal full-load current when first energized for a few cycles of the input current. The selection of over-current-protection devices, such as fuses and circuit breakers is made more complicated when high inrush currents must be tolerated.

For inrush current, according to [18], the time of the transient matters. It also depends on the point of the ac line-power voltage wave at which the power switch closes. Depending on the load switch, the inrush spike can be high, but at another point, it can be of lower or shorter duration. Point-on switching of the induction motor and capacitors in the network can reduce the inrush current using voltage and current zero and point-on crossing detection.

As recently as 1988, the only common method for reducing cage-rotor induction motor inrush current was the installation of starting resistors or star-delta starting. For starting resistors, they are connected in series and slowly reduced to reduce the net load impedance during switch-on; this is, however, not the best solution because resistors must be included in the circuit breaker design, which will require maintenance with switch arcing leading to wear. For start-delta starting, the IM is started with the windings in star, then reconnected in delta close to full load. Both of these methods give reduced starting torque as well as current. There can be a problem with false or unnecessary tripping of protection relays, which can affect power quality. There can also be damage, due to the use of soft starters [19]. These are the motivations for further study of the inrush and starting current phenomena [20–22].

The paper will first review some theory of the induction motor. It will use equivalent circuit analysis to assess the operation. The paper will then identify a number of motors and their parameters to highlight how, as the motors become larger, they tend to become more inductive. Experimental results will be put forward to validate the work.

2. Theory

2.1. Steady-State Equivalent Circuit Analysis

The use of equivalent circuits in electrical engineering is very well known. Indeed, Kron [23] published a comprehensive book on their use in electro-magnetic devices. The induction motor equivalent circuit was described well by Alger [24] in his well-known text. It is used here in the steady-state form using resistors and reactances. For a 3-phase IM, the standard per-phase equivalent circuit is illustrated in Figure 2a. This affects the operation of the machine, as shown in [25]. In the equivalent circuit:

R_1 is the stator winding resistance.

R_2' is the rotor resistance referred to the stator.

X_1 is the stator winding leakage reactance.

X_2' is the rotor leakage reactance referred to the stator.

X_m is the magnetising reactance.

R_c is the core loss resistance in the stator and rotor.

E_{ph} is the per-phase terminal voltage.

This is a per-phase model so the assumption is that if the motor is a three terminal black-box, the internal connection is star, no matter if it is connected internally as star or delta. If it is star, then reconnected in delta internally would reduce all the impedances in the per-phase equivalent circuit by three, and the rated voltage would go down by $\sqrt{3}$, while the rated current would go up by $\sqrt{3}$. These parameters can be obtained using the simple running-light and locked-rotor tests.

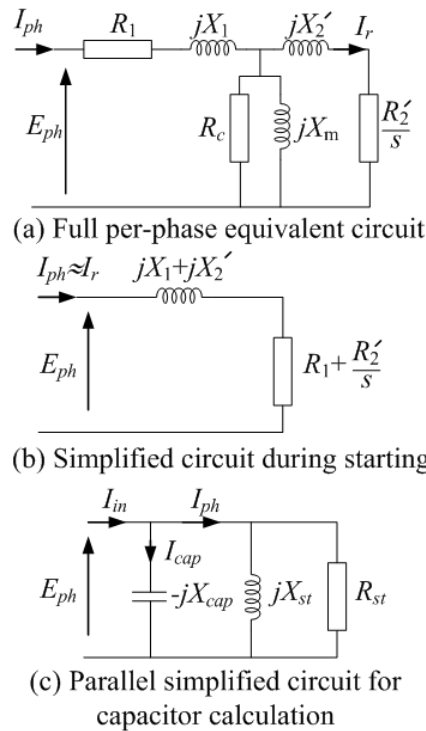


Figure 2. Equivalent circuits.

As stated above, the magnetizing reactance and core loss resistance are represented by X_m and R_c ; for a well-designed machine, these are much greater than the stator resistance R_1 and leakage reactance X_1 , and for the referred rotor components, the leakage reactance X_2' and resistance R_2'/s . The p.u. slip s is:

$$s = \frac{\omega_s - \omega_r}{\omega_s} \tag{1}$$

where the synchronous speed is ω_s and the motor speed is ω_r . The effective rotor resistance $\frac{R_2'}{s}$ is formed by the addition of the electro-mechanical energy conversion component and the rotor resistance, i.e.,

$$\frac{R_2'}{s} = \frac{(1-s)R_2'}{s} + R_2' \tag{2}$$

The copper loss in the rotor for a 3-phase motor is given by $3|I_r|^2 R_2'$ while the mechanical output power is:

$$\frac{3(1-s)|I_r|^2 R_2'}{s} \tag{3}$$

Using (3) and (1), the torque can be written as:

$$\begin{aligned} T_{mech} &= \frac{P_{mech}}{\omega_r} = \frac{3(1-s)|I_r|^2 R_2'}{s} \times \frac{1}{\omega_r} \\ &= \frac{3(1-s)|I_r|^2 R_2'}{s} \times \frac{1}{(1-s)\omega_s} = \frac{3|I_r|^2 R_2'}{s\omega_s} \end{aligned} \tag{4}$$

and:

$$I_r = I_{in} \times \frac{Z_m \left(\frac{R_2'}{s} + jX_2' \right)}{Z_m + \left(\frac{R_2'}{s} + jX_2' \right)} \tag{5}$$

where:

$$Z_m = \frac{jX_m R_c}{R_c + jX_m} \quad (6)$$

The torque/speed, current/speed, power/speed and reactive power/speed steady-state curves can be obtained by calculation using the equivalent circuit parameters.

2.2. Compensation During Starting

Z_m is formed from the parallel magnetizing components X_m and R_c and these are much greater than the other equivalent circuit parameters, so they can be neglected when $s \approx 1$ in Figure 2a. The approximate circuit in Figure 2b can then be used. When this approximation becomes invalid depends on the circuit X/R ratio. When high, i.e., very inductive, the speed will be close to the synchronous speed before the R'_2/s has an effect. In this case, the run-up current will be almost constant until close to full-load. This is a function of the IM but they generally become more inductive with increasing size. The later simulations will illustrate this. The circuit simplification in Figure 2b can be used in parallel with the compensation capacitors in order to calculate their capacitances. For the circuit in Figure 2c with unity slip:

$$R_1 + R'_2 + j(X_1 + X'_2) = \frac{jR_{st}X_{st}}{R_{st} + jX_{st}} \quad (7)$$

giving:

$$R_{st} = \frac{1}{(R_1 + R'_2)} \left((R_1 + R'_2)^2 + (X_1 + X'_2)^2 \right) \quad (8)$$

$$X_{st} = \frac{1}{(X_1 + X'_2)} \left((R_1 + R'_2)^2 + (X_1 + X'_2)^2 \right) \quad (9)$$

To obtain resonance, where I_{in} is real, in Figure 2c:

$$X_{cap} = X_{st} \quad (10)$$

Hence, the compensation capacitances can be calculated with ease.

2.2.1. Effects of Saturation

The induction motor can have substantial effects due to saturation, particularly during starting and for smaller motors with skewing on the rotor or stator that will cause axial saturation [26,27]. The models developed here are linear and do not account for saturation, since they use equivalent circuit analysis and motor tests. The locked rotor test is done at a reduced level if done manually, so it may not include saturation effects. For the industrial machines, the locked rotor test may be automated and done at a level where the saturation is incorporated into the equivalent circuit parameters.

Saturation will tend to reduce the motor impedance and increase the starting current and torque, generating "pull-up" torque where the torque increases from about $s = 0.5$ down to standstill where $s = 1$. Papers which address this are [28,29].

Analytical methods [30,31] and electromagnet finite element analysis [32] can be used to assess saturation in machines. Here, equivalent circuit models are used for machine performance assessment over a variety of machines.

2.2.2. Star or Delta Capacitor Connection

The compensation capacitors can be connected in either:

- Shunt capacitors;
- Series capacitor.

In this work, the capacitors are connected in shunt with the motor. There are some specific advantages of using shunt capacitors:

- They reduce the line current of the system;
- They can improve the voltage level of the load;
- They can reduce system losses;
- They can improve the power factor of the source current;
- Can reduce capital investment of the load because the supply may not need to be upgraded.

Obviously, these benefits come from the fact that the effects of the capacitor are to reduce the reactive current flowing through the whole system.

Series-connected capacitors for motors are not an appropriate application because they have to be very large and carry the full load current while their voltage is lower than for shunt-connected capacitors. This can potentially cause a catastrophic failure. For the series connection, capacitor failure can cause motor failure because it makes the load unbalanced; therefore, the motor may be damaged due to the unbalanced voltage and possible 2-phase operation, causing overheating [33,34].

Series connected capacitors are more vulnerable to failure due to harmonics [35,36], since they have to carry the full motor current.

2.2.3. Capacitor Filters

Delta connection is chosen in this work. They provide capacitance to each phase. However, they can be susceptible to low frequency harmonics and filters may be necessary [37]. These are shown in Figure 3. A low-pass filter should be suitable in this application to suppress the 5th, 7th, 11th, 13th, etc. harmonics.

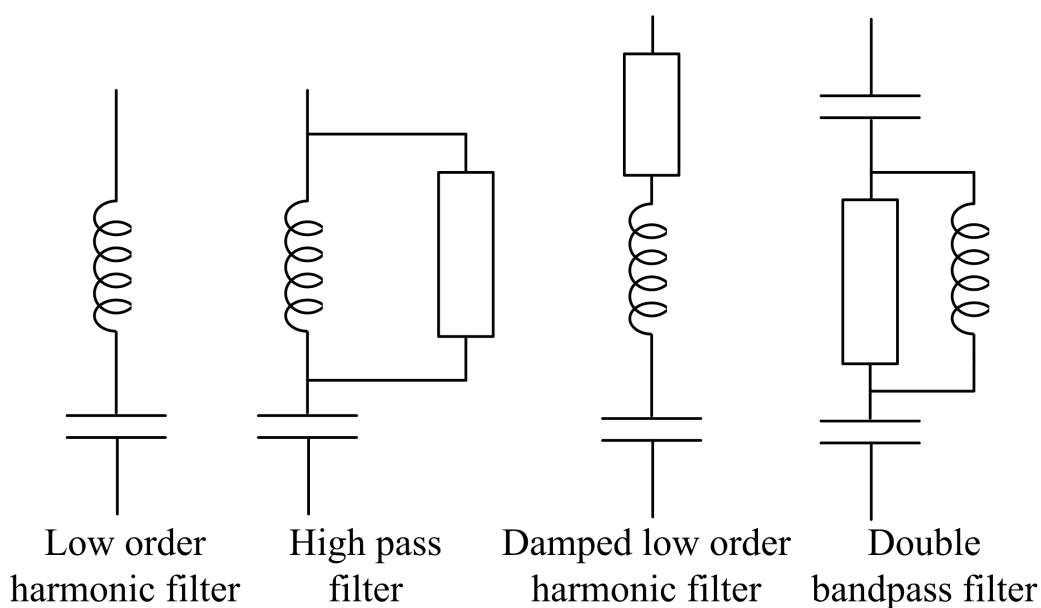


Figure 3. Possible filter arrangements—low pass filter most suitable in this application.

2.2.4. Capacitor Failure

In the case of a failure of one capacitor cell for one phase for any reason, it moves from a closed delta to an open delta configuration [38,39], as illustrated in Figure 4. In this case, the voltage remains unchanged. When in delta, if a capacitor is lost, the other two will continue to deliver reactive power, whereas they will produce less reactive power if they were connected in star. In Figure 4, if they normally produce 10 kVAr at 600 V, when a delta-connected capacitor is lost, then two will continue to produce 20 kVAr in total. However, in star, they are now series connected across two phases so that the capacitor voltage goes down from $\frac{600}{\sqrt{3}}$ to $\frac{600}{2}$. The reactive power in a capacitor is $Q = I^2 X_c = \frac{V^2}{X_c}$.

Taking voltage-squared ratios, then $Q_{tot} = 2 \times 10 \times \left(\frac{\sqrt{3}}{2}\right)^2 = 15 \text{ kVAR}$. When there is a capacitor open-circuit, the other two will supply reactive power to the system than a star-connected network as shown in Figure 4.

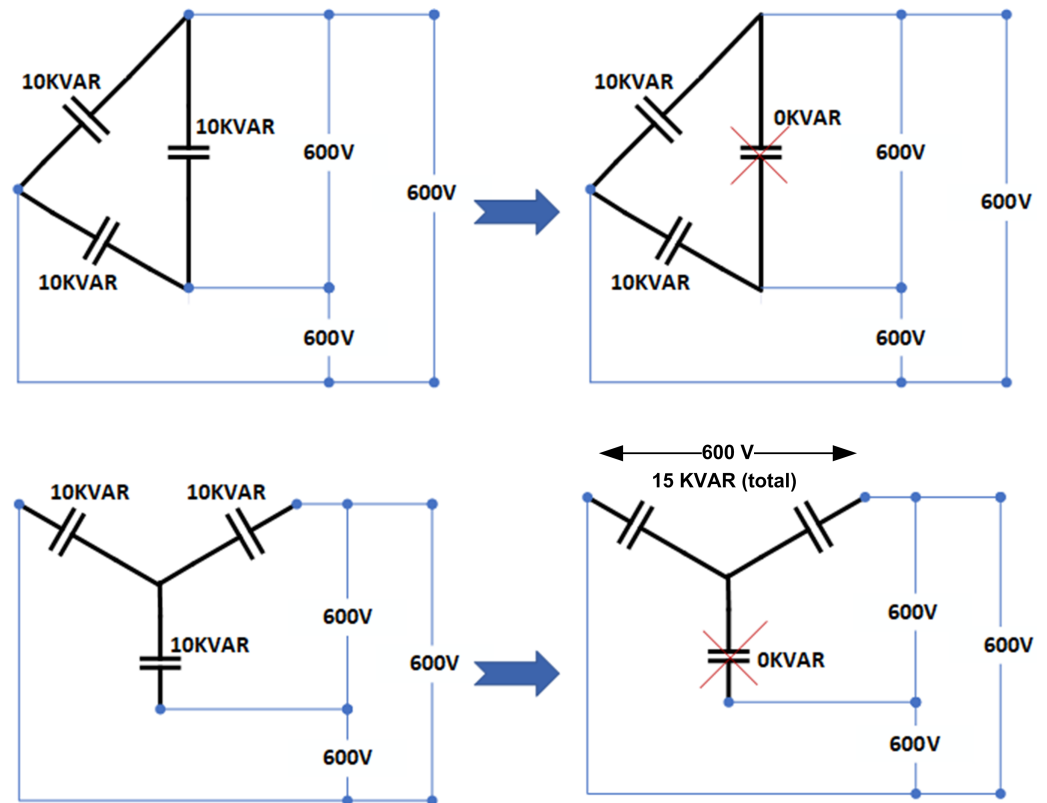


Figure 4. Failure of a capacitor in a star or delta connected bank.

2.3. Steady-State Run-Up Time

Using equivalent circuit analysis, the speed or slip can be stepped through to obtain current, torque, power, reactive power, etc., against speed or slip. It is useful for the motor torque to be matched against a load to get results against time as the motor runs up to speed. This can be done by considering the electro-mechanical system to estimate the run-up time then the torque equation can be used. That is:

$$T_{mech} = T_{load} + T_{FW} + J \frac{D\omega_m}{dt} \tag{11}$$

where J is the inertia and ω_m is the motor speed in rad/s. The load torque T_{load} and friction and windage torque T_{FW} may take the general form:

$$T = K_1 + K_2\omega_m + K_3\omega_m^2 \tag{12}$$

The coefficients will vary greatly. For instance, a positive displacement pump requires a constant torque given constant output pressure, so K_1 will be dominant (and the power proportional to the speed [40]), whereas a large fan has a torque that is mostly a function of the square of the speed (with the power a cubic function) so that the K_3 is dominant [41].

If the motor is started with no load, for instance with no fluid flowing in the pump, then the system inertia can be used to find the approximate run-up time. This means:

$$T_m = J \frac{d\omega_m}{dt} \tag{13}$$

when stepping through the slip and calculating the torque, the time step can also be calculated from:

$$\Delta t \approx J \frac{\Delta \omega_m}{T_{mech}} \tag{14}$$

For a set step in speed $\Delta \omega_m$ then:

$$\Delta t(n) \approx \frac{2J\Delta \omega_m}{(T_{mech}(n) + T_{mech}(n - 1))} \tag{15}$$

This uses the mean torque between steps $n - 1$ and n . If there is a load then this can be included as:

$$\Delta t(n) \approx \frac{2J\Delta \omega_m}{(T_{mech}(n) - T_{load}(n) + T_{mech}(n - 1) - T_{load}(n - 1))} \tag{16}$$

The time at each step can then be obtained by numerical summation of the time steps:

$$t(n) = \sum_1^n \Delta t(n) \tag{17}$$

2.4. Complete System

Figure 5 illustrates the full system with the capacitor connection in a delta together with the 3-phase induction motor. The practical realization of this is given in Section 5.

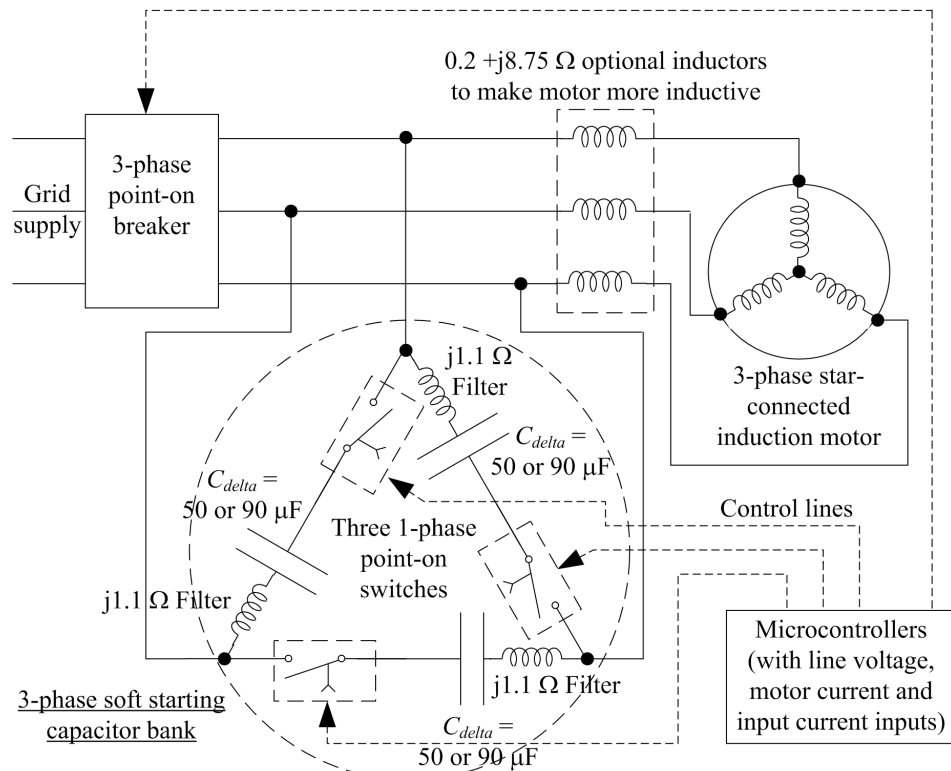


Figure 5. Complete system power circuit.

3. Motor Models

This section puts forward seven machines that represent a broad spectrum of induction motors and includes the experimental machine. They are presented in terms of their ratings and per-phase equivalent circuit parameter.

3.1. Parameters for Different Machines

Seven IMs were investigated to highlight their various characteristics. These are over a wide range of power, voltage and pole number.

The first is a small 1.5 kW 346 V 4-pole laboratory machine. The equivalent circuit parameters were obtained through running-light and locked-rotor tests.

There are four commercial machines from Valiadas. We used a 1.5 kW, 400 V, 4-pole, 50 Hz machine for comparison with the laboratory machine, a 45 kW, 400 V, 4-pole, 50 Hz machine, as an example of a larger LV machine. A 200 kW, 3300 V, 2-pole machine was used as an example of a higher-speed MV machine, and then a 1 MW 6000 V 6-pole was used as an example of a larger MV low speed motor. The data was obtained from data sheets and test reports, obtained through the company website [42]. To further add machines to the mix two example machines were analyzed by Sen [43] and these are 60 Hz examples to give variation. There is a small 3.75 kW, 440 V, 4-pole, 60 Hz machine and a very large 3.75 MW, 6900 V, 12-pole, 60 Hz machine that were used as an example of a very large MV machine.

These machines present a wide range of machines and their parameters are put forward in Table 1. They were simulated to assess their performance.

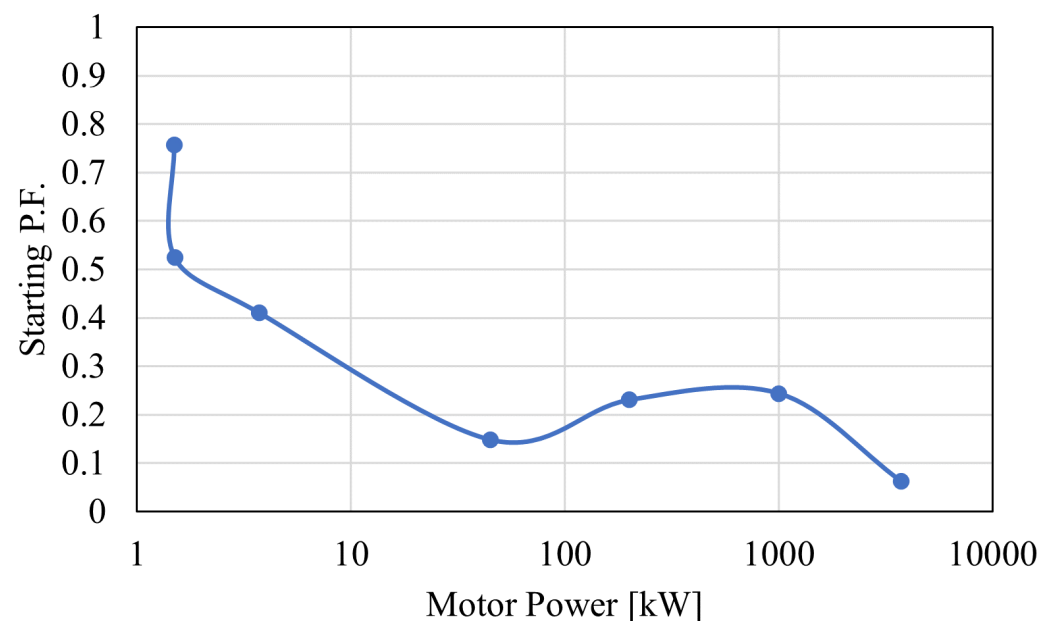
Table 1. Motor parameters.

No.	Machine	kW	V_{Line} [V]	I_{Line} [A]	Poles	f_s [Hz]	rpm	J [kg·m ²]
1	Lab machine	1.5	220	5.8	4	50	1425	0.012
2	Valiadas K90L-4	1.5	400	3.3	4	50	1440	—
3	Sen 5 HP	3.75	440	3.73	4	60	1753	0.05
4	Valiadis K200L-4	45	400	81.1	4	50	1480	0.246
5	Valiadas KHV355-2	200	3300	44.4	2	50	—	2.6
6	Valiadas TMKHV560-6	1000	6000	110	6	50	990	79
7	Sen 5000 HP	3730	6900	358	12	60	596	145.47

The per-phase equivalent circuit parameters, as obtained from the sources or measured through testing, are listed in Table 2. The X/R ratio is the starting reaction/resistance ratio; it can be noted that larger machines are more inductive at the start, when compared to the smaller machines. The starting power factors are shown in Figure 6, and these confirm the general trend of the power factor at the start, decreasing with increasing size. Obviously this is very much a function of the motor design but the power range of the machines studied probably covers the whole range of available three-phase induction motors. Note that the power is on a logarithmic scale.

Table 2. Motor equivalent circuit parameters (values in Ω).

No.	Machine	X_m	R_c	R_1	R'_2	$X_1 + X'_2$	X/R
1	Lab machine	58	81	2.13	1.34	2.99	0.86
2	Valiadas K90L-4	115.2	1568.2	1.325	3.87	8.44	1.62
3	Sen 5 HP	110	900	1.2	1.5	6.0	2.22
4	Valiadis K200L-4	5.13	178.1	0.059	0.013	0.48	6.67
5	Valiadas KHV355-2	118	1333	0.79	0.57	5.75	4.2
6	Valiadas TMKHV560-6	102.5	900.0	0.97	0.24	4.78	3.97
7	Sen 5000 HP	46.0	600.0	0.083	0.080	2.60	15.95

**Figure 6.** Power factor start for different motors.

3.2. P.U. Parameters

The actual parameters in Table 2 can be used for the simulations; however, for direct comparison, the parameters can be converted into p.u., as shown in Table 3. The normalization is done using:

$$Z_{in}(1 \text{ p.u.}) = \frac{V_{Line}(\text{rated})}{\sqrt{3}I_{Line}(\text{rated})} \quad (18)$$

The p.u. values for $R_1 + R'_2$ and $X_1 + X'_2$ are plotted against motor power in Figure 7. Note that both axes are logarithmic. It can be seen that $X_1 + X'_2$ is generally constant across the logarithmic scale with the 1.5 kW lab machine being an outlier, whereas $R_1 + R'_2$ varies with a general trend downwards with increasing motor power.

In Figure 8, X_m and R_c are plotted. Again, both axes are logarithmic. The magnetizing reactance X_m stays almost steady with a slight upward trend with increasing power. The core loss resistance is much larger with the same upward trend; however, the lab machine is again an outlier with the core loss resistance being much lower.

Table 3. Motor equivalent circuit parameters (values in p.u.).

No.	Machine	$Z_{in}[\Omega]$	X_m	R_c	R_1	R'_2	$X_1 + X'_2$
1	Lab machine	37.478	1.54	2.17	0.0568	0.0357	0.080
2	Valiadas K90L-4	69.98	1.65	22.41	0.189	0.0554	0.121
3	Sen 5 HP	36.29	3.03	24.8	0.0331	0.0413	0.165
4	Valiadis K200L-4	2.85	1.80	62.56	0.0207	0.0046	0.169
5	Valiadas KHV355-2	42.91	2.75	31.08	0.0184	0.0314	0.134
6	Valiadas TMKHV560-6	29.11	3.5	40.00	0.0332	0.0082	0.164
7	Sen 5000 HP	11.13	4.13	53.92	0.0075	0.0072	0.234

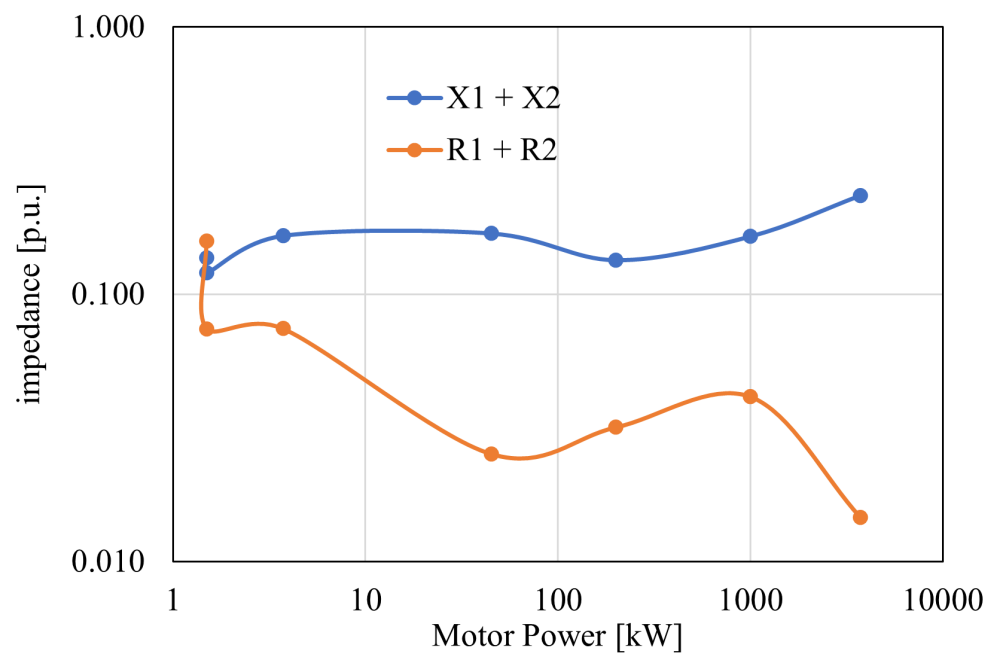


Figure 7. p.u. input resistances and reactances at start for different motors.

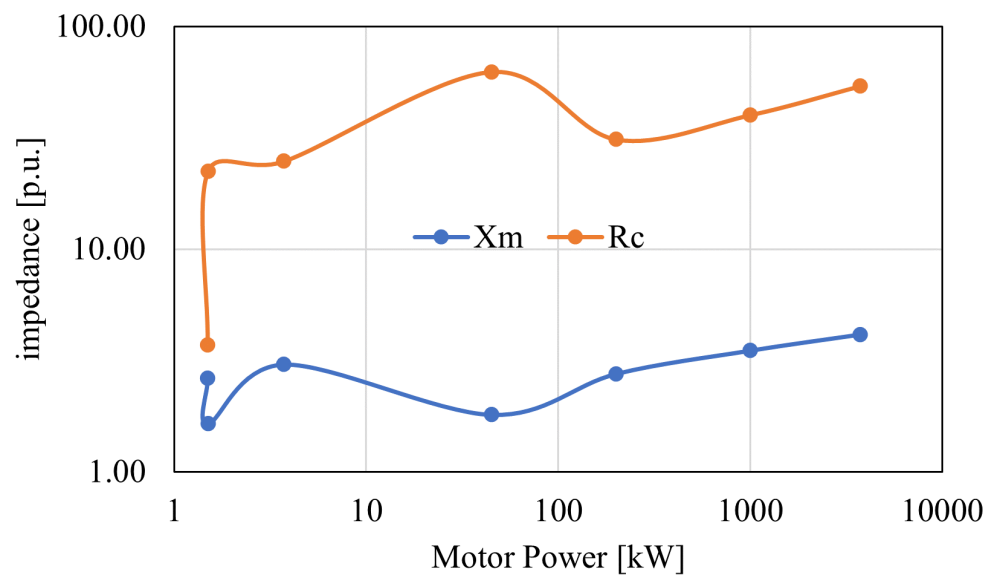


Figure 8. Variation of P. U. X_m and R_c for different motors.

4. Steady-State Equivalent Circuit Analysis Method for Assessing Capacitor Compensation

In this section, the machines were simulated with a capacitor to assess the efficacy of the method using steady-state equivalent circuits to step through the speed range. For the figures for each machine, the run-up current and torque were first put into graph (a). This includes a load torque and friction and profile from (12) using the full load point. The first full load point was obtained using the torque speed curve by moving back from the no load point until $P_m(\text{rated}) = T_m \omega_r$. At this point, the rated slip was s_{fl} . From this, the load torque is:

$$\begin{aligned} T_l(s) &= T_m(\text{rated}) \left(K_1 + K_2(1 - s + s_{fl}) + K_3(1 - s + s_{fl})^2 \right) \\ T_l(s) &= T_m(\text{rated}) \left(0.05 + 0.1(1 - s + s_{fl}) + 0.85(1 - s + s_{fl})^2 \right) \end{aligned} \quad (19)$$

This means that the speed-squared coefficient K_3 is 85% of the total torque at rated speed, the speed coefficient K_2 is 10%, and the constant coefficient K_1 is 5%. This may be reasonable for a smaller machine attached to a pump or a fan, but for a large machine, often the dominant term is K_3 , which approaches 100% or the machine is started with no load where it only has to overcome the inertia and friction and windage terms (for instance, for a pump, the fluid supply-side valve is kept closed until it runs up to speed, then it is opened).

Power and reactive power are given in the motor figures in graph (b) and this shows how inductive the machine is across the speed range. The delta-connected parallel compensation capacitance required to correct the power factor during starting to unity is given in (c). The total input current to the motor and compensation capacitors are shown in (d), and this was done for three capacitances—the values calculated at start, then with half this capacitance and then the third capacitance. This is because the required capacitance decreases with speed, so that the selection of the capacitors is, to some extent, a compromise. Each machine was simulated.

4.1. Motor No. 1: 1.5 kW 220 V Lab Machine

This experimental machine is not very inductive, as can be seen in Figure 9b where the power was greater than the reactive power. Consequently, in Figure 9c, it can be seen that only a reduction of about 25% was possible. The machine was tested at a reduced voltage and, to increase its inductance, additional reactances were added to make it behave more like a large machine.

Run-Up Time at 100 V No-Load for Experiments

The experiments were conducted at 100 V to reduce stressing on the system. A further calculation could be done using (15) and setting the inertia to 0.012 kg m^2 , as given in Table 1. The run-up time is shown in Figure 10 to be about 0.55 s. Furthermore, the PEAK currents when 50 μF and 100 μF delta-connected capacitors are used to correct the current are also shown. It can be seen that the capacitors should be switched out after 0.35 s if a timer is used and it starts on no load. However, this time would be extended if there is load. A centripetal switch could be used, and Figure 9d shows that this should be about 1250 rpm, in this instance.

4.2. Motor No. 2: 1.5 kW 400 V Valiadas K90L-4

As previously stated, this is a commercial machine and it is more reactive when starting compared to Motor No. 1. It can be seen in Figure 11c that the required capacitance varies considerably over the speed range. In Figure 11d, it can be seen that using 94 μF capacitors offers a 50% reduction in starting current, but needed to be switched out below 1000 rpm. Better operation across the whole range occurred using 47 μF , which would be switched out at 1200 rpm.

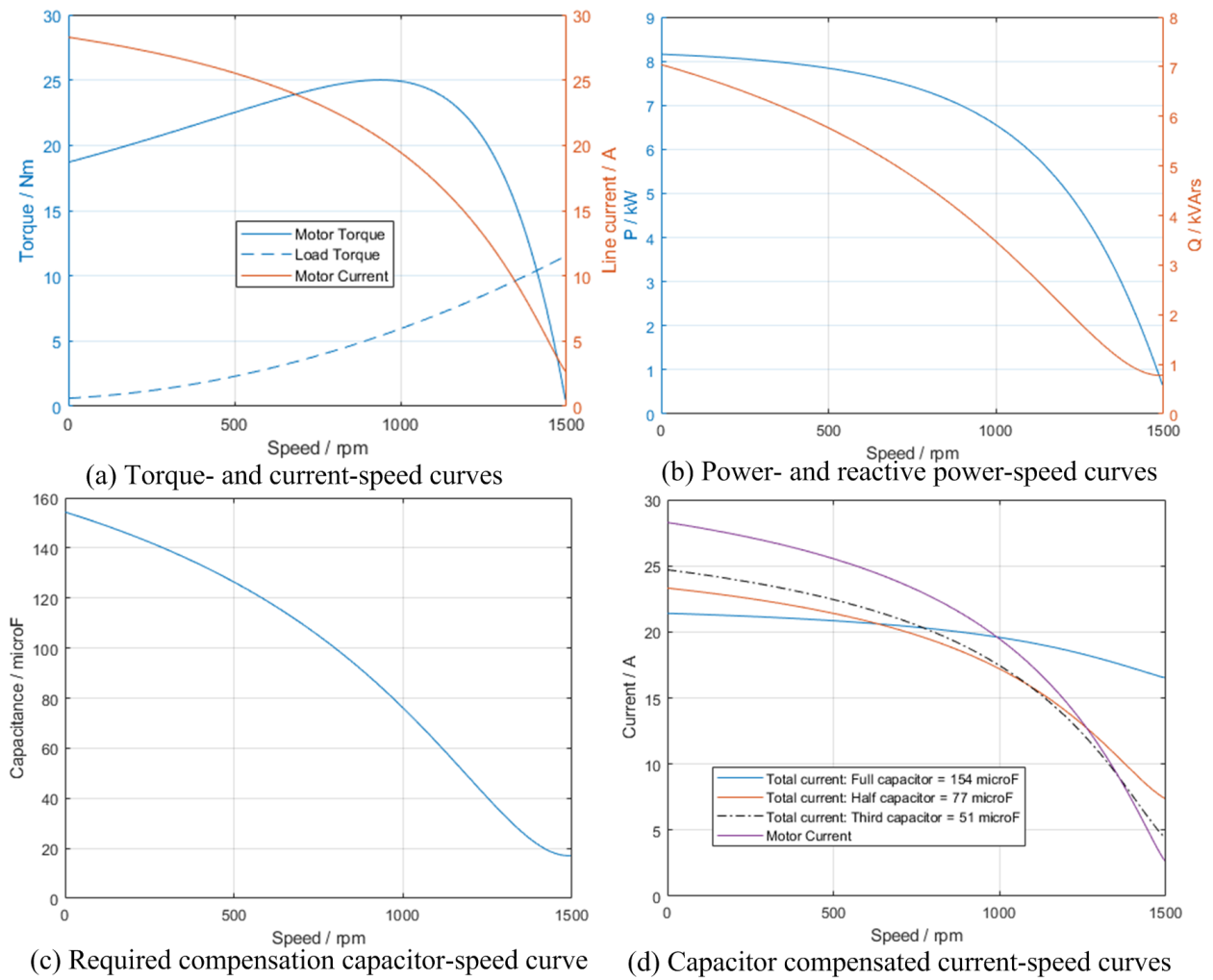


Figure 9. Motor No. 1: Comparison of 1.5 kW 220 V lab machine capacitor compensation starting.

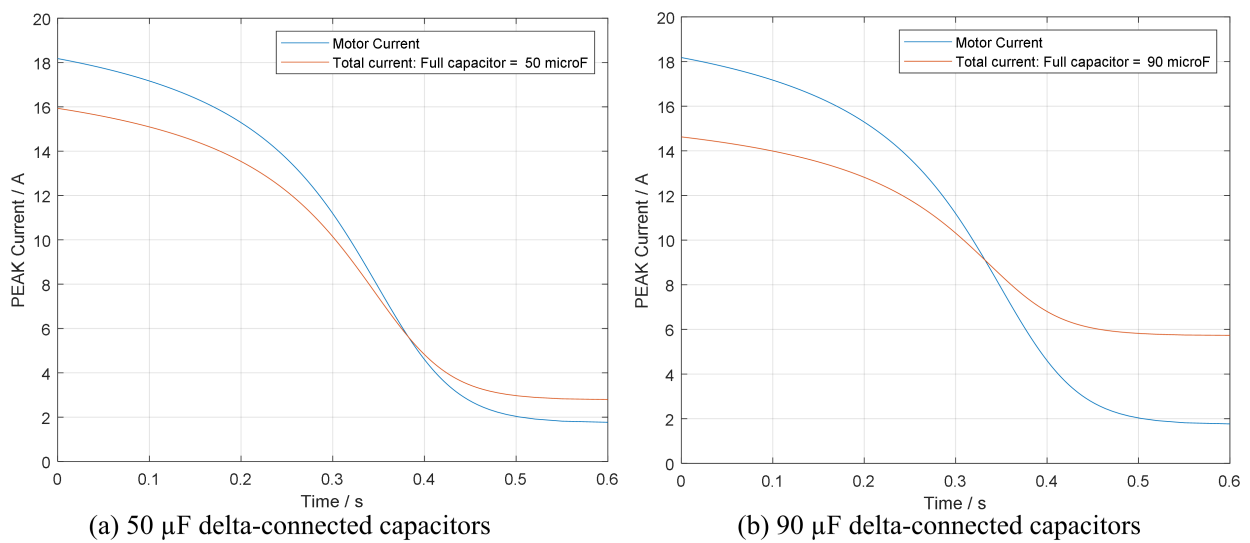


Figure 10. Motor No. 1: Run-up time prediction for experimental machine at 100 V—currents with 50 μF and 90 μF .

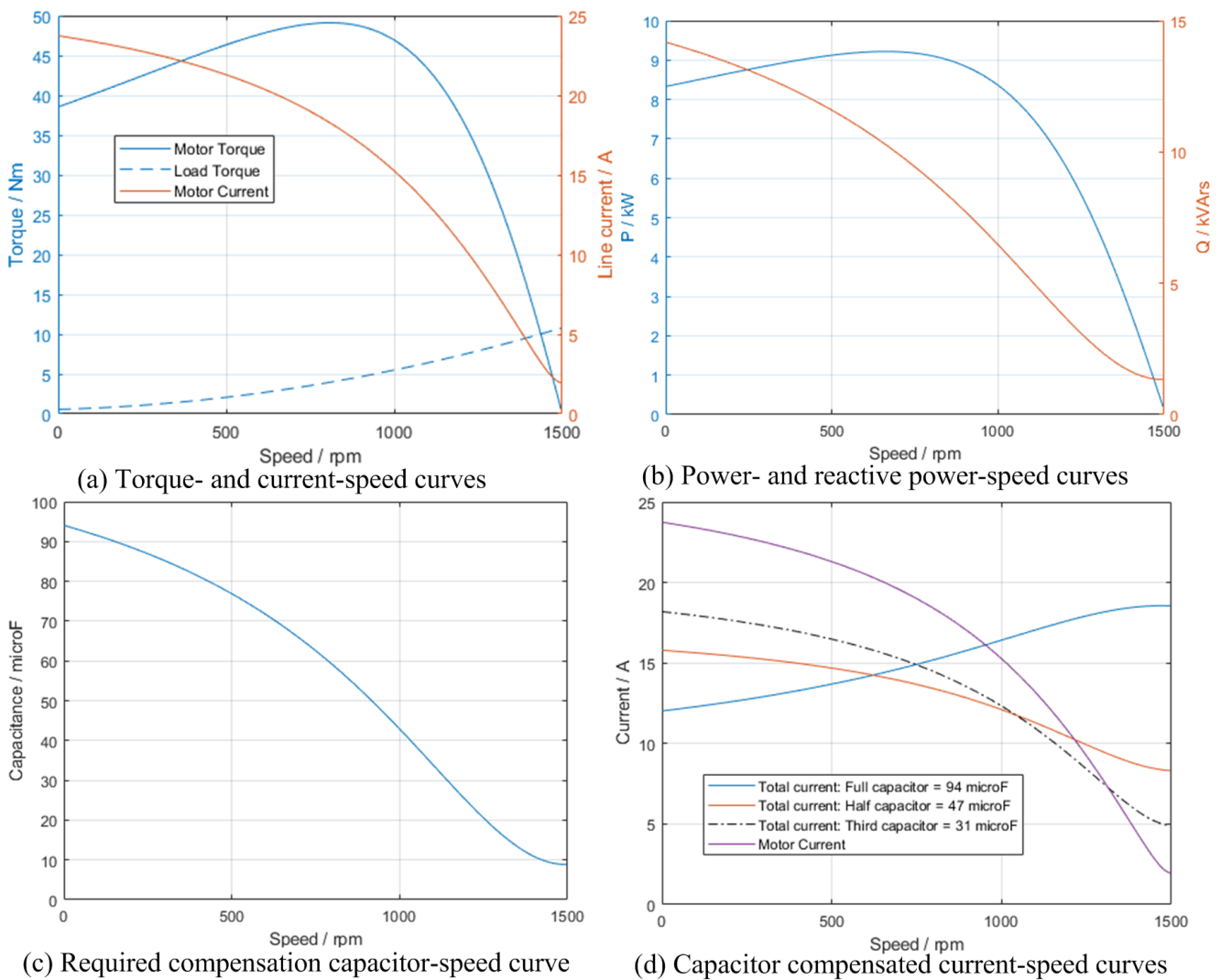


Figure 11. Motor No. 2: Comparison of 1.5 kW 400 V Valiadas K90L-4 machine capacitor compensation starting.

4.3. Motor No. 3: 3.75 kW 440 V Sen 5 HP

This is a small 4-pole machine operation at 440 V and the capacitance requirement in Figure 12c still varied considerably across the speed range. In Figure 12b, it can be seen that the reactive power was higher than the power at start but the reactive power decreased until the power was higher at about 1300 rpm (note the different scales on the left and right axes and that it is a 60 Hz machine so that the synchronous speed was 1800 rpm). If 62 μF capacitors were used, then the starting current was reduced by 38%, which should be switched out at 1600 rpm. Again, using the capacitance calculated at start led to a value that was too high because the current increased and the power factor began to lead.

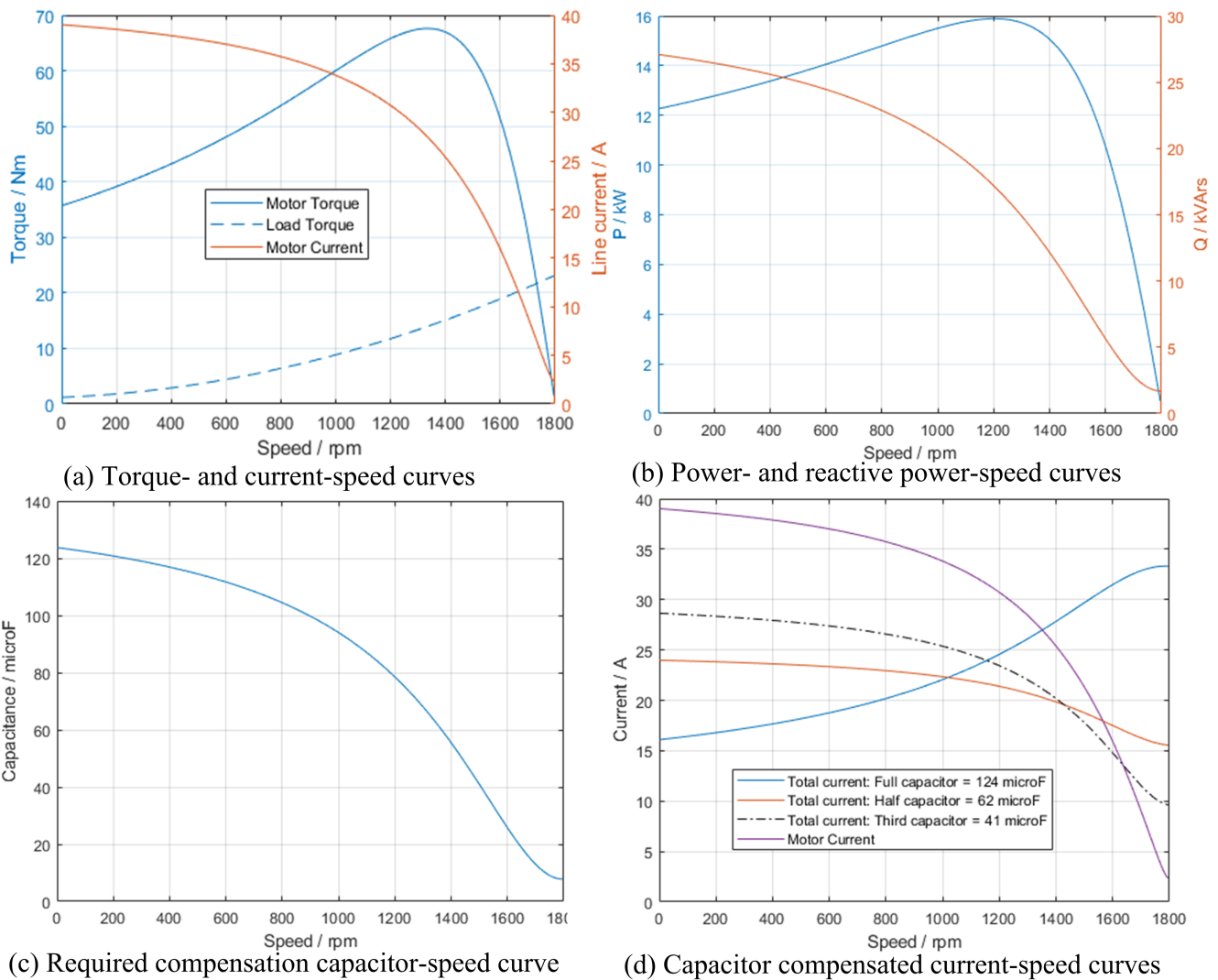


Figure 12. Motor No. 3: Comparison of 3.75 kW 440 V Sen 5 HP machine capacitor compensation starting.

4.4. Motor No. 4: 45 kW 400 V Valiadis K200L-4

As previously mentioned, this machine can be considered as a large machine for the 400 V rating; this means a high current rating. The required capacitance in Figure 13c was shown to be nearly constant across the speed range. This illustrates that this method is more suitable for large machines. However, because it is a low voltage, high current machine, the required capacitance was high at 2.21 mF at the starting point. This reduced the starting current by 85%, though there was a peak of 325 A close to the steady-state operating point, when the capacitors should be switched out to avoid the current increasing further and the system operating with a leading power factor. If 1.15 mF capacitors were used for the capacitance, then they gave nearly a 50% reduction, without the peak being close to the synchronous speed. This may be a better compromise, since it does not need accurate control of the capacitor switch-out.

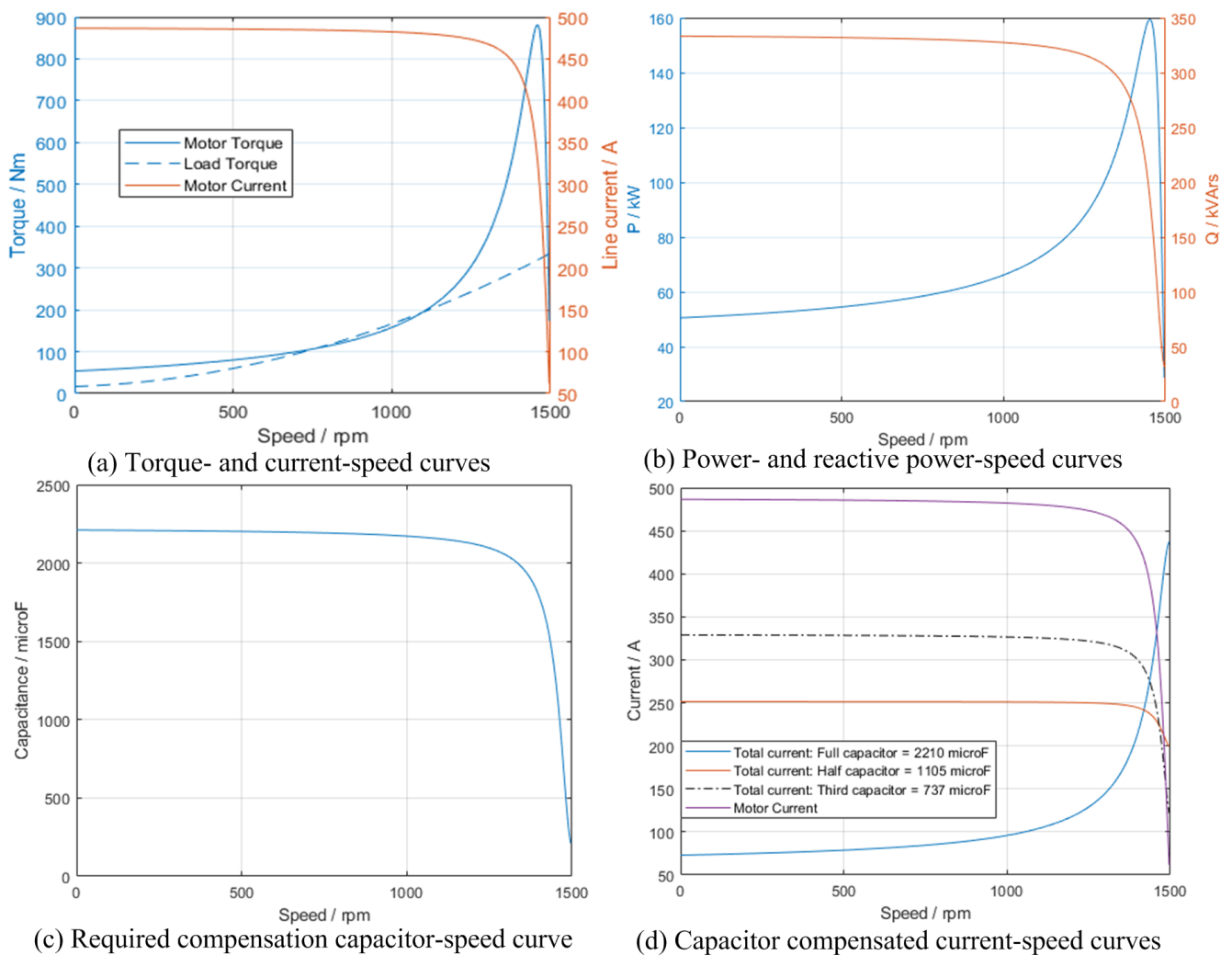


Figure 13. Motor No. 4: Comparison of 45 kW 400 V Valiadis K200L-4 machine capacitor compensation starting.

Run-Up Time at Rated Voltage and No Load

This is a repeat of timed run-up for the 1 MW machine in Section 4.6; however, the machine does not produce sufficient torque to overcome the load used. If this is changed to $K_1 = K_2 = 0$ and $K_3 = 1$ the motor can start. This is illustrated in Figure 14. It can be seen, though, that the motor torque is only just greater than the load torque at about 1000 rpm. Therefore, it would be recommended that this motor be started with no load.

The run up has to be conducted with some sort of load, which could simply be the inertia and the load being a squared function of the speed $K_3 = 1$. The inertia is given as 0.246 kg m^2 , but the machine will possibly be attached to a pump or fan. To accommodate this, the inertia was doubled so that $J = 0.246 \times 2 = 0.492 \text{ kg m}^2$. The run-up is shown in Figure 15 and takes approximately 2.8 s. However, in Figure 14, it was marginal as to whether this machine would start with a load, then a simulation could be carried out with no load, as shown in Figure 16. Then, the run up time was much faster at 0.75 s.

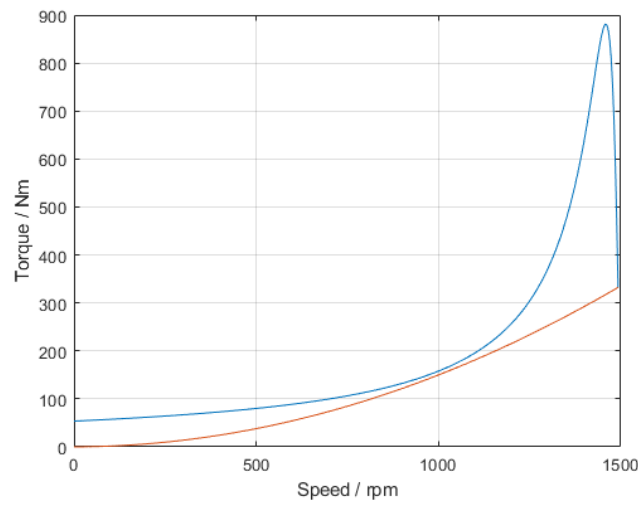


Figure 14. Motor No. 4: Speed-torque curve of 45 kW 400 V Valiadis K200L-4 machine and load torque with $K_3 = 1$. Blue line is motor torque, brown line is load torque.

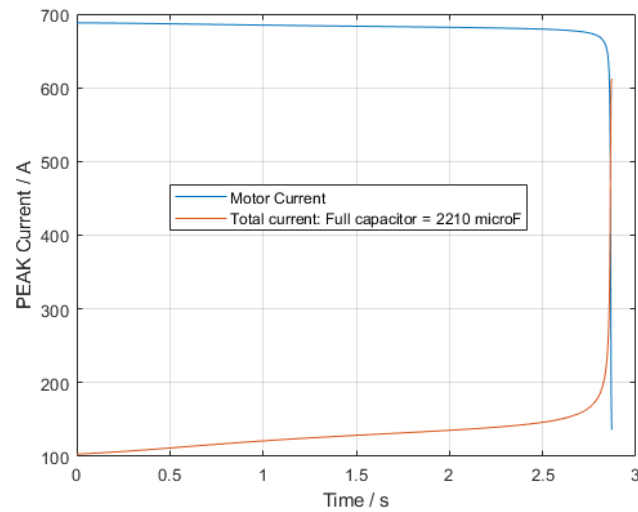


Figure 15. Motor No. 4 : Speed-time curve of 45 kW 400 V Valiadis K200L-4 machine with inertia of 0.492 kgm^2 and speed-squared load torque function $K_3 = 1$.

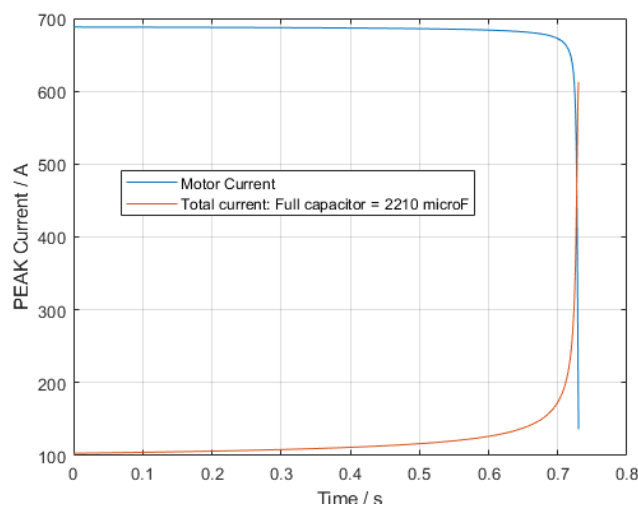


Figure 16. Motor No. 4: Speed-time curve of 45 kW 400 V Valiadis K200L-4 machine with inertia of 0.492 kgm^2 and no load.

4.5. Motor No. 5: 200 kW 3300 V Valiadas KHV355-2

This is a small- to medium-sized machine for the voltage rating. As shown in Figure 17, the starting current could be reduced by 77% using 177 μF capacitors, though this would increase to a peak of 225 A at 2750 rpm, where the capacitors should be switched out to avoid the grid current increasing further. If 88 μF capacitors were used, then the starting current is halved to 175 A and there is no peak current. Again, this may be a better compromise solution not requiring accurate capacitor turn-off.

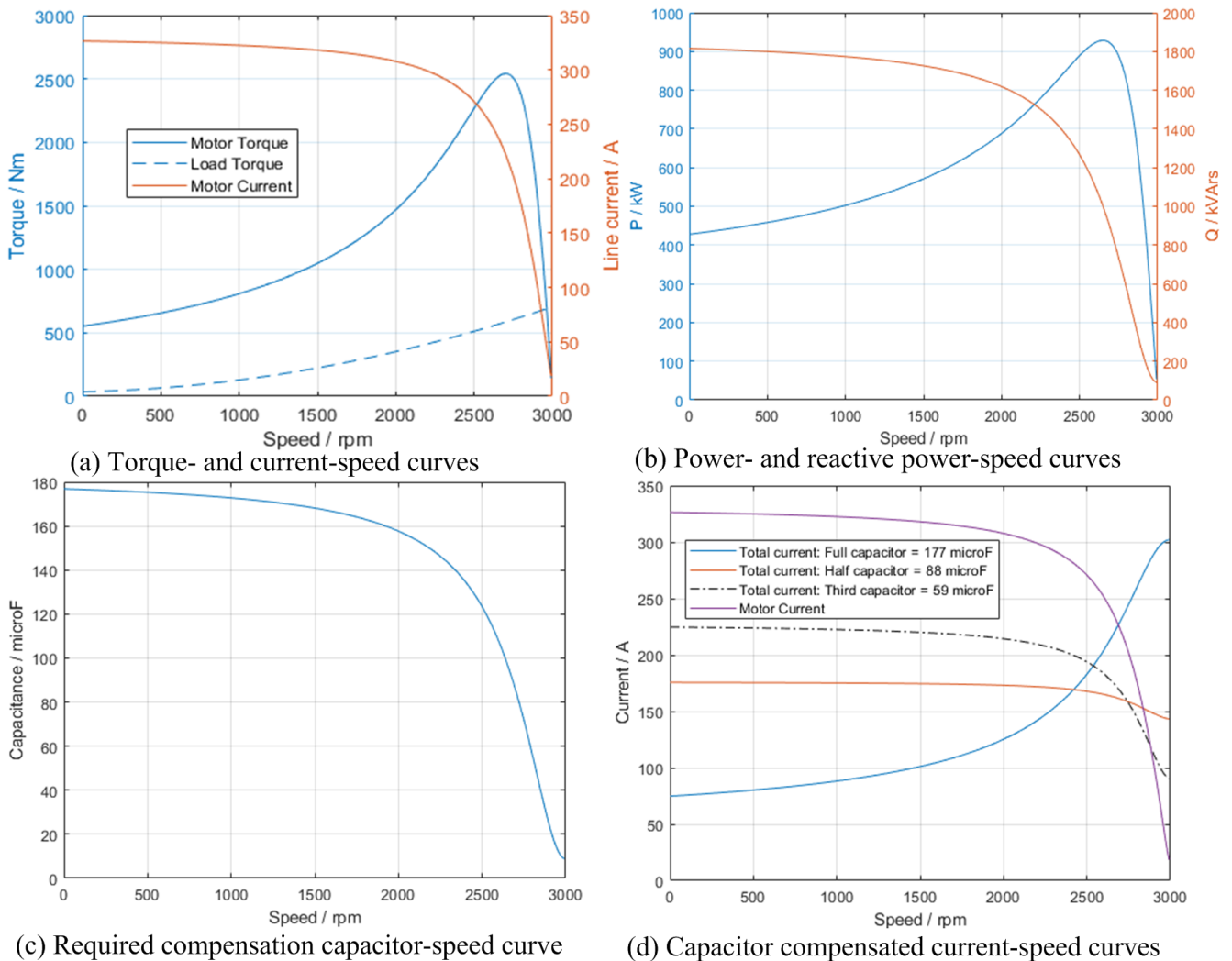


Figure 17. Motor No. 5: Comparison of 200 kW 3300 V Valiadas KHV355-2 machine capacitor compensation starting.

4.6. Motor No. 6: 1 MW 6000 V Valiadas TMKHV560-6

This is a large machine for the voltage rating. As with Motor No. 4, the required capacitance was nearly constant across much of the speed range, this is shown in Figure 18. Using 211 μF capacitors could reduce the current by 73% at the start, but the current would rise to two-thirds of the starting motor current at about 950 rpm when the capacitors should be switched out to prevent further increase in current. If 105 μF was used, then a 45% reduction was possible with no peak current before capacitor turn-off.

Run-Up Time at Rated Voltage and Load

To show the speed of a large machine running up to speed, then a simulation was carried out at the rated voltage of 6000 V. A further calculation could be done using (16) and setting the inertia to 79 kg m^2 , as given in Table 1. The run-up time is shown in Figure 19 to be about 2.5 s, showing that large machines can take time to run up to speed. Furthermore, shown is the current when 221 μF delta-connected capacitors were used to correct the current. It can be seen that they can be disconnected very close to the full load speed. With the load removed, the run-up time reduces, as shown in Figure 20.

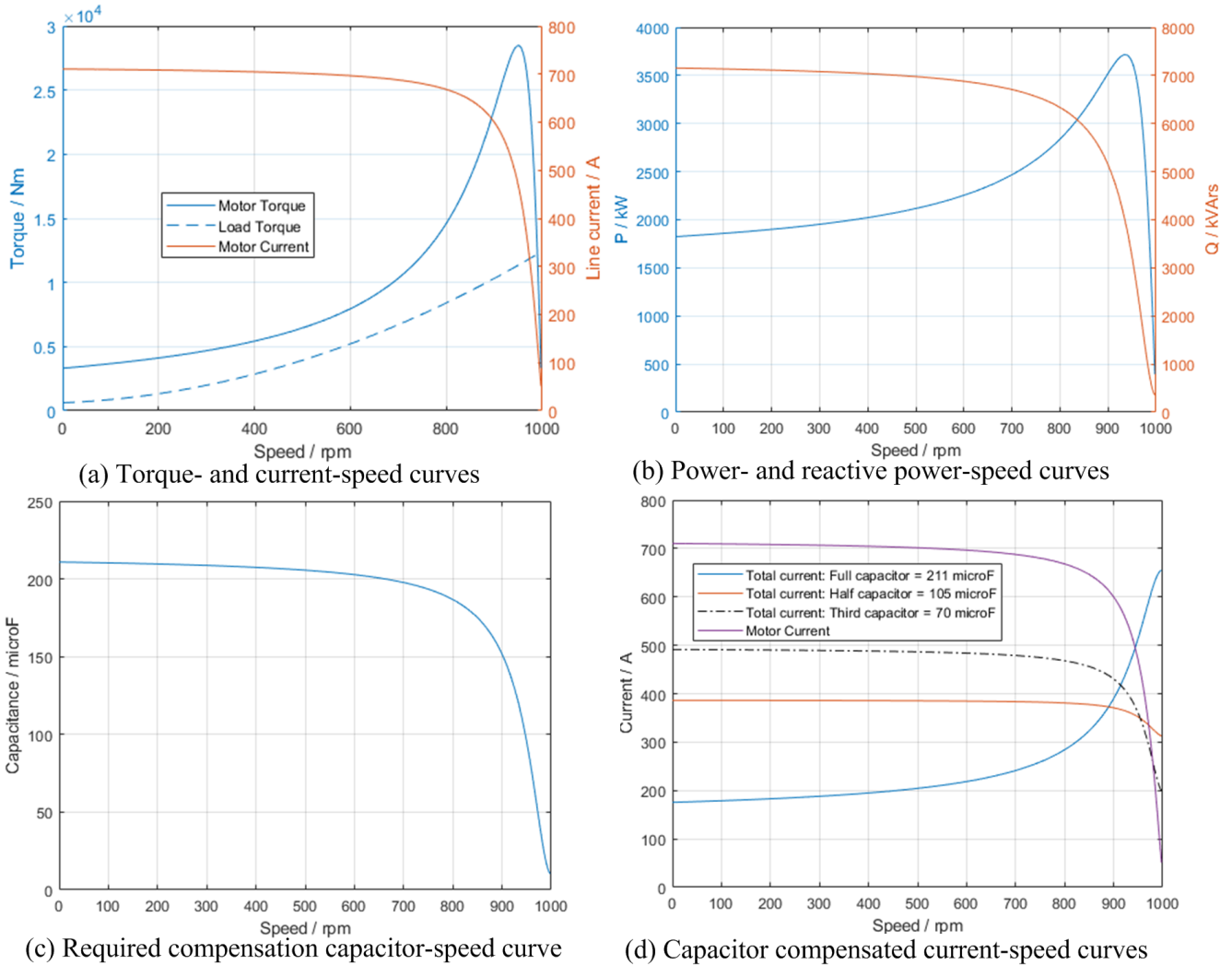


Figure 18. Motor No. 6: Comparison of 1 MW 6000 V Valiadas TMKHV560-6 machine capacitor compensation starting.

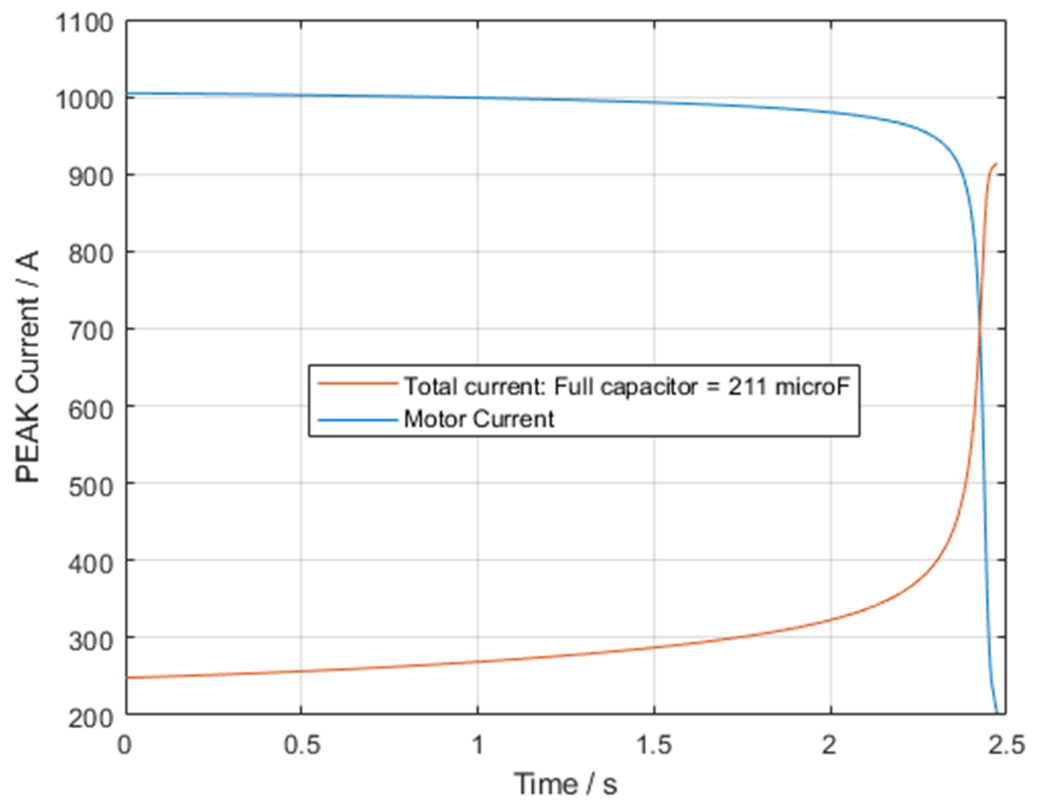


Figure 19. Motor No. 6: Run-up time prediction for PEAK current for 1 MW machine at rated voltage and with load.

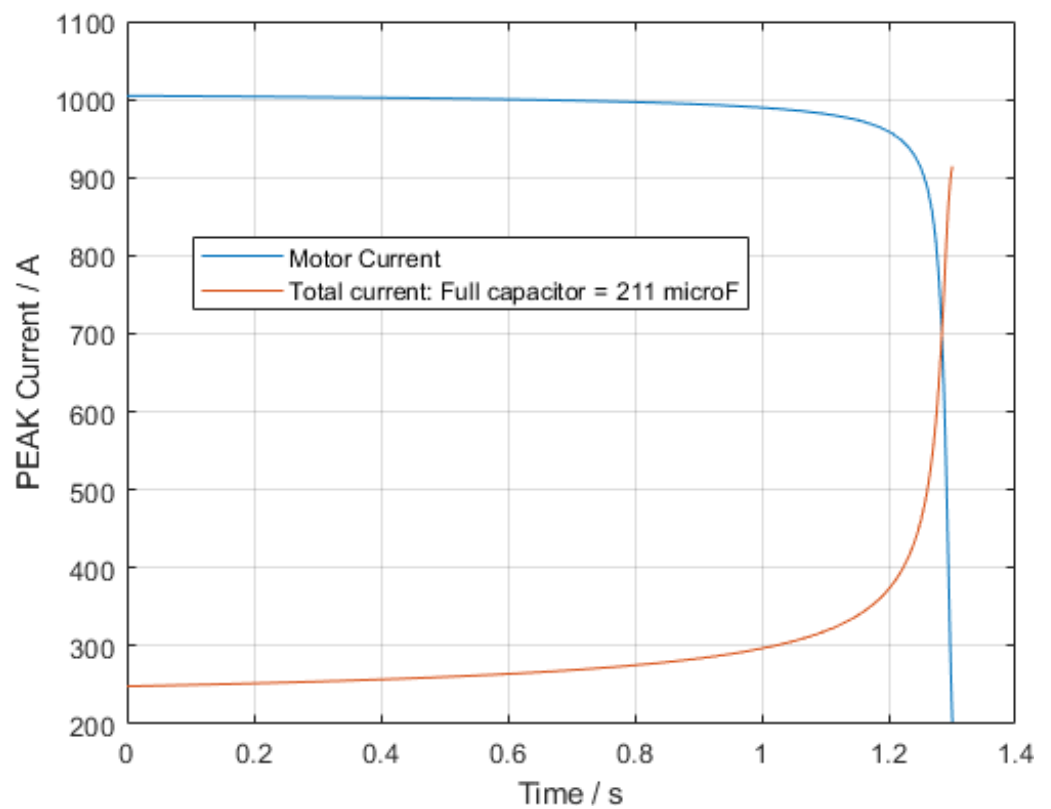


Figure 20. Motor No. 6: Run-up time prediction for PEAK current for 1 MW machine at rated voltage and with no load.

4.7. Motor No. 7: 3.75 MW 6900 V Sen 5000 HP

This is a large high-efficiency machine with low starting torque. The starting current could be reduced by 90%, as shown in Figure 21d using 343 μF capacitors, with a peak of 1100 A (71% of the motor starting current) just before capacitor turn off. This would need careful control, since it is close to the full load speed. The run-up current is halved if 172 μF capacitors are used, and there is no peak current.

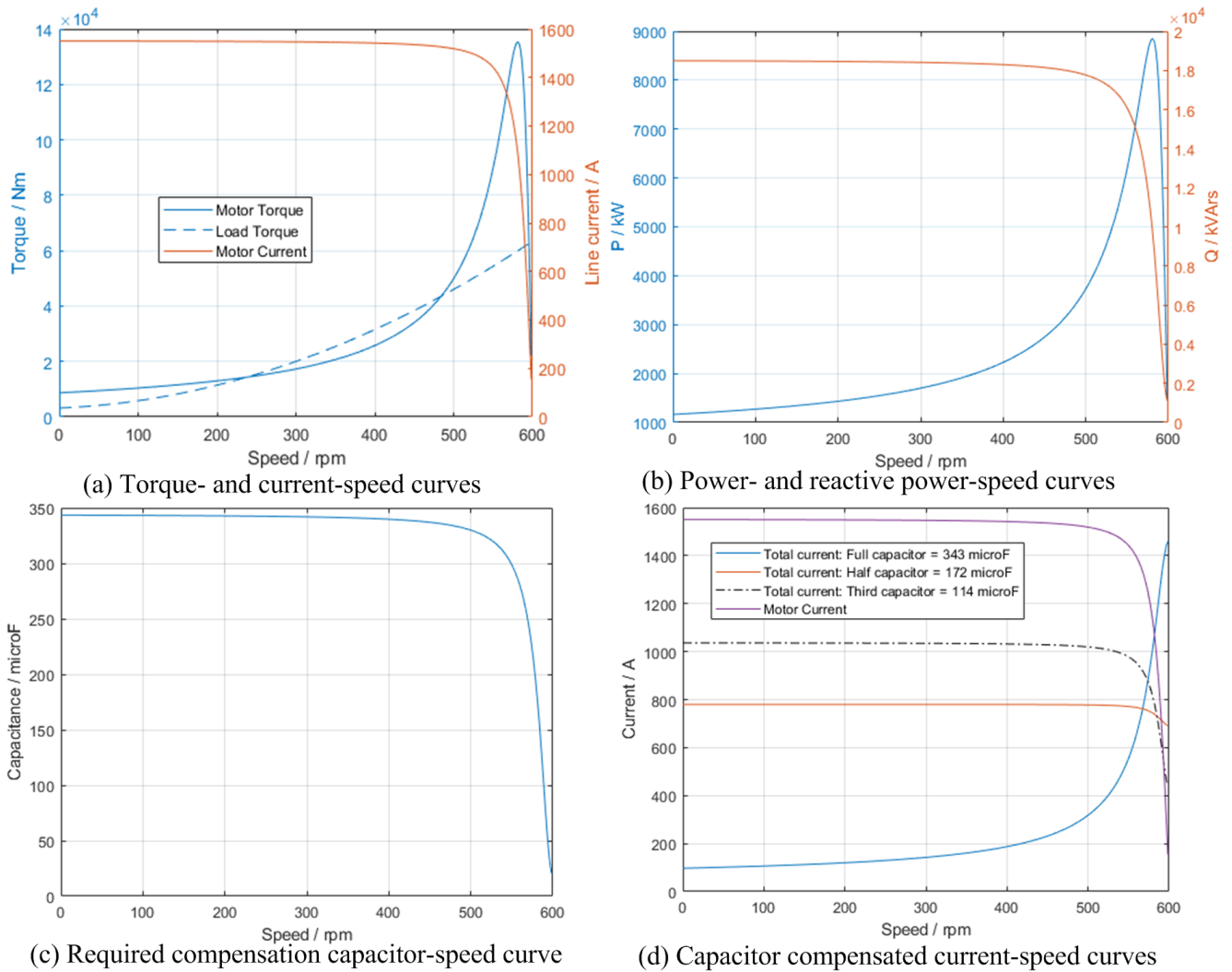


Figure 21. Motor No. 7: Comparison of 3.75 MW 6900 V Sen 5000 HP machine capacitor compensation starting.

Run-Up Time at Rated Voltage and No Load

This is a repeat of timed run-up for the 1 MW machine. The machine will not start the load in that simulation. Indeed, even if the load was changed to $K_1 = K_2 = 0$ and $K_3 = 1$, there was still a mid region where the load torque was greater than the motor torque, which would prevent run up. This is illustrated in Figure 22.

The run up had to be conducted with no load, however, there would be inertia. It is given as 145.47 kg m^2 , but the machine would possibly be attached to a pump or fan. To accommodate this, then the inertia was doubled so that $J = 145.47 \times 2 = 290.94 \text{ kg m}^2$. The run-up is shown in Figure 23 and took approximately 1.1 s. In reality, this would be much higher since the inertia may well be much higher, and there was no friction, windage or any other loading in the simulation.

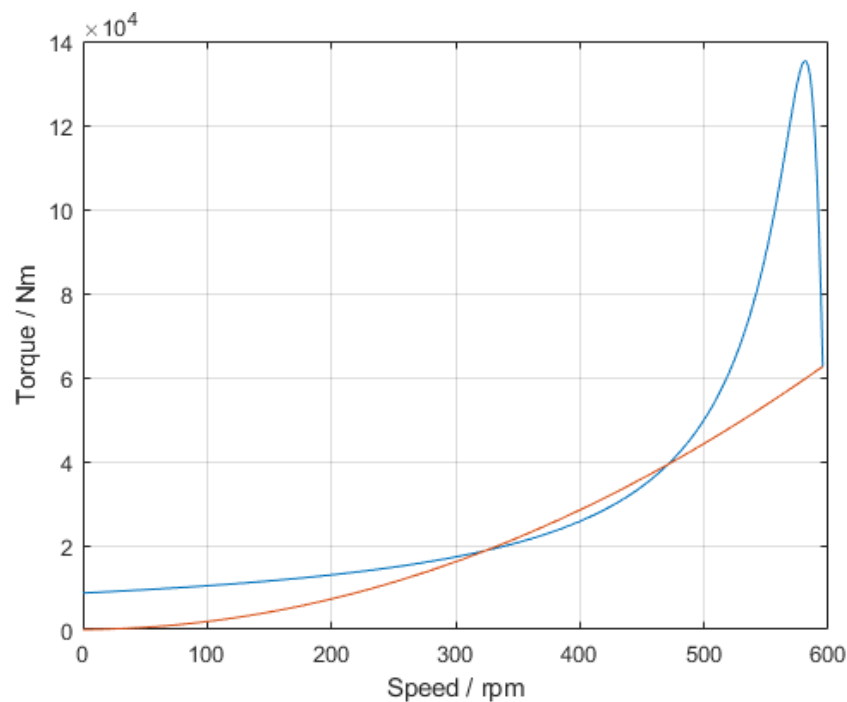


Figure 22. Motor No. 7: Speed-torque curve of 3.75 MW 6900 V Sen 5000 HP machine and load torque with $K_3 = 1$. Blue line is motor torque, brown line is load torque.

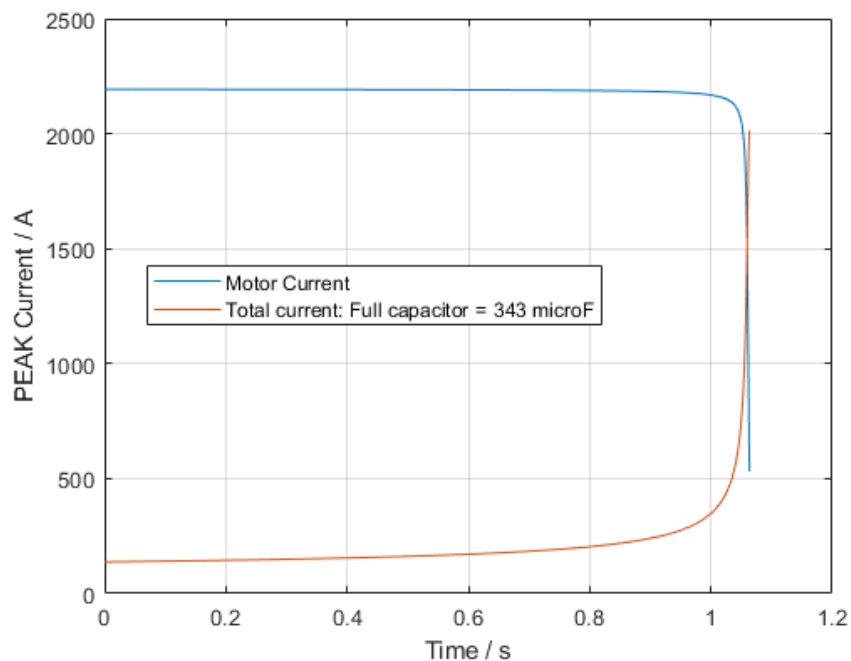


Figure 23. Motor No. 7: Speed-time curve of 3.75 MW 6900 V Sen 5000 HP machine inertia of 290.84 kg m^2 and no load.

4.8. Discussion on Simulations

In the simulations section, seven motors were simulated and the results compared. Figures 7 and 8 give the P.U. values for the equivalent circuit parameters and the stator and rotor resistances generally go down with increasing size while the leakage reactances, together with the magnetizing reactances and core loss resistances go up. This makes the larger motors more reactive at start and through run-up.

Figures 9, 11–13, 17, 18 and 21 give the same comparative results for Motor Nos. 1 to 7 against speed as the slip is stepped down from 1 to 0. These figures show the torque and

current curves, then the power and reactive power curves, the required capacitors C_{unity} to correct the current drawn to unity and then a set of currents for capacitor compensation using C_{unity} , $C_{\text{unity}}/2$ and $C_{\text{unity}}/3$. For comparison, Motor Nos. 1 to 3 can be classed as low power machines for their voltage ratings and this method of starting is not very advantageous as shown in the results, though could offer some starting assistance if tuned properly. The choice of capacitor is very much a compromise since C_{unity} changes greatly across the speed range. However, Motor No. 4 is a 45 kW 400 V machine and can be classed as a large induction motor at this voltage rating and capacitor compensation does offer a good way to start the motor. Motor No. 5 is a 3300 V machine and at 200 kW is a medium-sized machine for this rating. Capacitor compensation offers improved starting. Motor No. 5 (1 MW 6000 V) and 6 (3.75 MW 6900 V) are large machines and this starting method does seem to offer a much improved starting performance if the capacitors are tuned correctly and switched out at the correct time.

4.9. Experimental Validation—Motor No. 1E Simulations

During the experiments, it was found that Motor No. 1 was not sufficiently inductive to give meaningful results for capacitor compensation. To address this, the 8.75Ω reactances were added to the machine. In the simulations, this was an additional 23.6 mH added to the stator leakage reactance so that the machine had an equivalent circuit that matched a larger machine, with it being more inductive during the run-up. The voltage was increased for this machine because it was found that with the added motor inductors, the machine would not run up to speed with a line voltage of 100 V rms, which is 141 V peak. The phase voltage was now set to 100 V peak, which gives a line voltage of 173 V peak or 122.5 V rms.

This section gave the steady-state simulations for this modified machine for comparison to the experimental results. The machine uses 90 μF compensation capacitors. The steady-state simulation for the motor and grid currents are shown in Figure 24.

During the experimental work, it was found that the machine ran up much slower than the simulations that had low load and used the inertia as the main mechanical load. By simulation experiment, it was found that the 5 s run-up time could be achieved by adding a friction torque of 0.625 Nm, and this is shown in Figure 25. The machine is old with little maintenance and this seems to be a reasonable addition to the load profile.

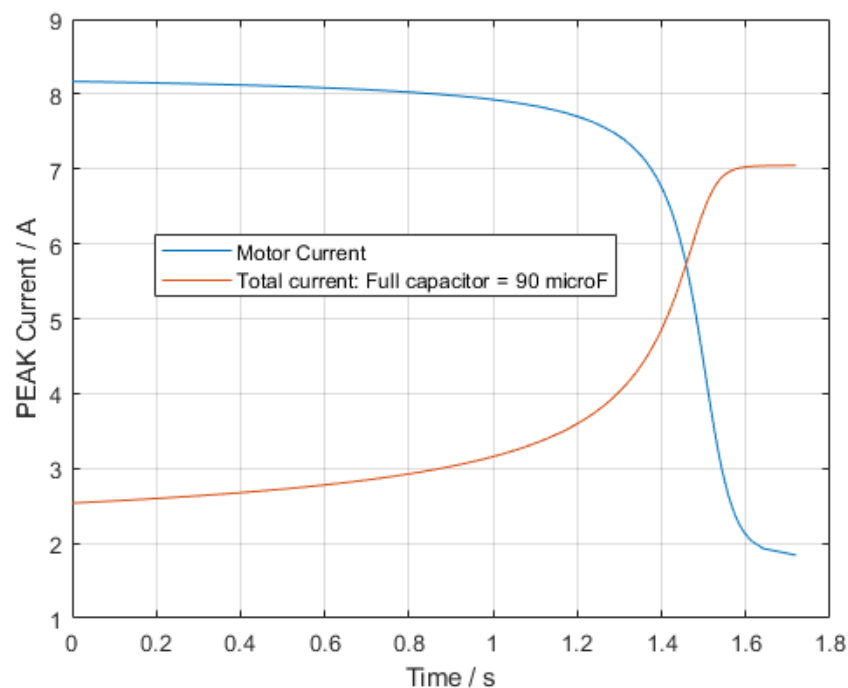


Figure 24. Motor No. 1E steady-state simulation with 90 μF capacitors.

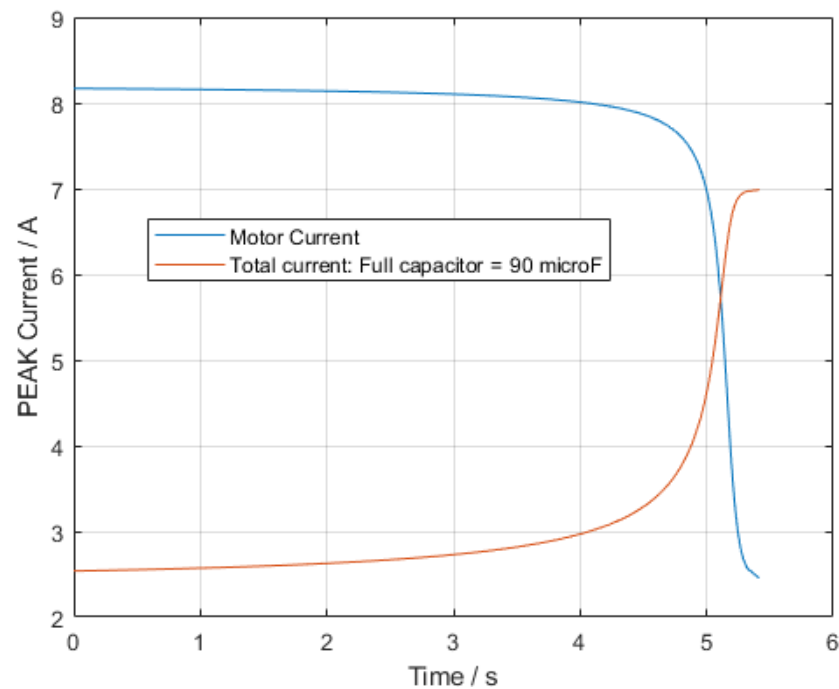


Figure 25. Motor No. 1E steady-state simulation with 90 μF capacitors switching and 0.625 Nm of friction added.

5. Experimental Setup

The final hardware is shown in Figure 26. The circuit connection is shown in Figure 5. The single-phase point-on switch connected to the induction motor were fitted for separate control of the capacitors, as shown in Figure 5. The three-phase point-on switch allowed for separate switching of phases and these were the main breakers (as shown in Figure 27) used in the point-on switching work with the capacitors and induction motor hard-wired in parallel.

In Figure 26 there are several capacitors in use. These are standard AC motor capacitors used to start single phase motors or compensate for a three-phase system and could be used to form a 50 μF or 90 μF delta connection. Motor No. 1 had inline inductors added to give a more inductive motor when starting. These were $0.2 + j8.75 \Omega$, which matched Motor No. 1 well and were available. In addition, smaller inductors were needed for capacitor filtering. These had impedances of $j1.1 \Omega$ (at 50 Hz) and represented a reasonable filter value for the 7th harmonic of the capacitors used. Section 6.3.1 gives a calculation of the harmonic impedance for the capacitors.

Solid-state breakers were used in the work—one three-phase breaker and three one-phase breakers. Solid-state breakers were used in the work—one three-phase breaker and three single-phase breakers, as shown in Figure 27. While the control for the three-phase breaker was only one signal as indicated, the switches will work in order when there is a zero crossing voltage point, so two phases were close and then the next 90° later.

This experimental setup was achieved by using a PIC MICROCONTROLLER 18F45K22. There were three main parts to this experimental switching arrangement, the current sensing, voltage sensing, and point-on switching control.

The commissioning involved testing individual subsystems before integrating them to operate as a complete control unit with sensor circuit subsystems, including the variable power supply used (an autotransformer) in the rig. For testing, a Fluke 435 Series II Three-Phase Power Quality and Energy Analyzer was used.

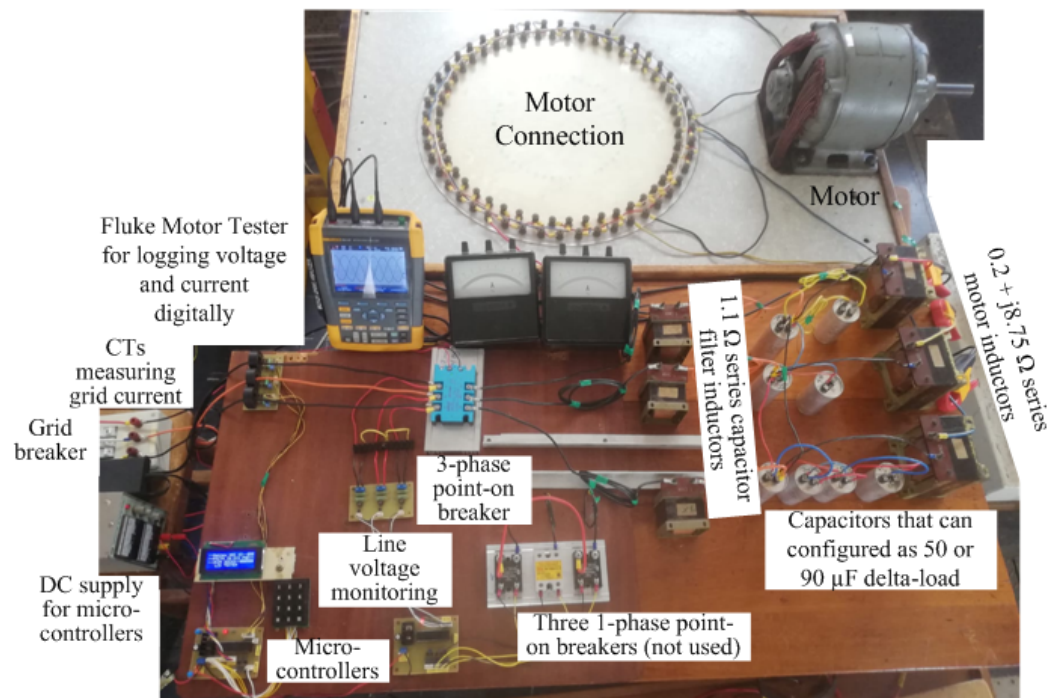


Figure 26. Final layout of test rig.



Figure 27. Solid state breakers used.

6. Experimental Results

This section validates the use of capacitor compensation experimentally using Motor Nos. 1 and 1E. The results investigate the run-up current and its reduction using capacitors and the transient turn using point-on switches, which turn on when the voltage across them is zero.

The use of series inductors with the capacitors was addressed to illustrate the harmonic filtering of low frequency harmonics.

The section first addresses capacitor compensation of Motor No. 1 and the change in grid current during locked rotor and running light tests. This was found to not produce good results, so Motor No. 1E was used and found it gave better illustration of capacitor compensation with locked rotor.

Transient experiments were then done, first with just parallel 90 μF capacitors and then with random turn-on to show the harmonic capacitor currents and transient turn-on current spikes. Low-pass filters were added to the capacitors formed from inductors, which were shown to improve the capacitor current. Finally point-on switching was carried out using the system designed for this project, and these show an improvement in transient current turn-on.

6.1. Initial Motor No. 1 Steady-State Testing—Locked-Rotor and Running-Light Tests

The initial testing for Motor No. 1 was conducted at 46 V and 100 V line; however, only the 100 V results are reported. Figure 10 gives the simulations and Tables 4–7 give the locked rotor and running light measured currents (using a digital multimeter). The three line currents were measured and the average was taken. These were converted to peak currents and the simulation peak currents (I_{Sim}) are given for comparison. It can be seen that for the locked rotor tests, the measured current was a little lower than predicted and the attenuation of current using the capacitors was not as substantial. This was even more noticeable at no load, as can be seen in Table 7. The capacitors did not appear to be supplying a high current. To address this, the waveforms were inspected, as shown in Figure 28. While the waveforms look reasonable in (a) and (b) at the locked rotor, it can be seen in (c) and (d) for the running-light tests, that there was substantial harmonic content in the line currents when the capacitors were connected; even without the capacitors, there appeared to be a degree of low frequency harmonics due to saturation in the motor. At this point, there was no filtering using the in-line inductors with the capacitors. It was decided to add inductance to the induction motor, so that it is more inductive and more representative of a larger machine.

Table 4. Motor No. 1 locked rotor test with and without 50 μF compensation capacitors—the peak measured current ($I_{mean\text{peak}}$) reduction was less than the simulated ($I_{Sim\text{peak}}$) current reduction.

100 V Line 50 μF Caps.	I_a	I_b	I_c	$I_{mean\text{rms}}$	$I_{mean\text{peak}}$	$I_{Sim\text{peak}}$
Motor	11.53	11.66	11.3	11.50	16.26	18.18
Capacitors and motor	11.22	11.39	10.96	11.19	15.83	15.93

Table 5. Motor No. 1 locked rotor test with and without 90 μF compensation capacitors— I_{mean} peak reduction was less than I_{Sim} peak current reduction.

100 V Line 90 μF Caps.	I_a	I_b	I_c	$I_{mean\text{rms}}$	$I_{mean\text{peak}}$	$I_{Sim\text{peak}}$
Motor	11.18	11.3	11.09	11.19	15.83	18.18
Capacitors and motor	10.45	10.59	10.36	10.47	14.80	14.62

Table 6. Motor No. 1 running light test with and without 50 μF compensation capacitors— I_{mean} peak reduction was less than I_{Sim} peak current reduction.

100 V Line 50 μF Caps.	I_a	I_b	I_c	$I_{mean\text{rms}}$	$I_{mean\text{peak}}$	$I_{Sim\text{ peak}}$
Motor	0.95	1.07	0.79	0.94	1.32	1.75
Capacitors and motor	0.34	0.59	0.5	0.48	0.67	2.75

Table 7. Motor No. 1 running light test with and without 90 μF compensation capacitors— I_{mean} peak reduction was less than I_{Sim} peak current reduction.

100 V Line 90 μF Caps.	I_a	I_b	I_c	$I_{mean\text{ rms}}$	$I_{mean\text{peak}}$	$I_{Sim\text{ peak}}$
Motor	0.91	1.03	0.8	0.91	1.29	1.75
Capacitors and motor	0.86	0.95	1.04	0.95	1.34	5.75

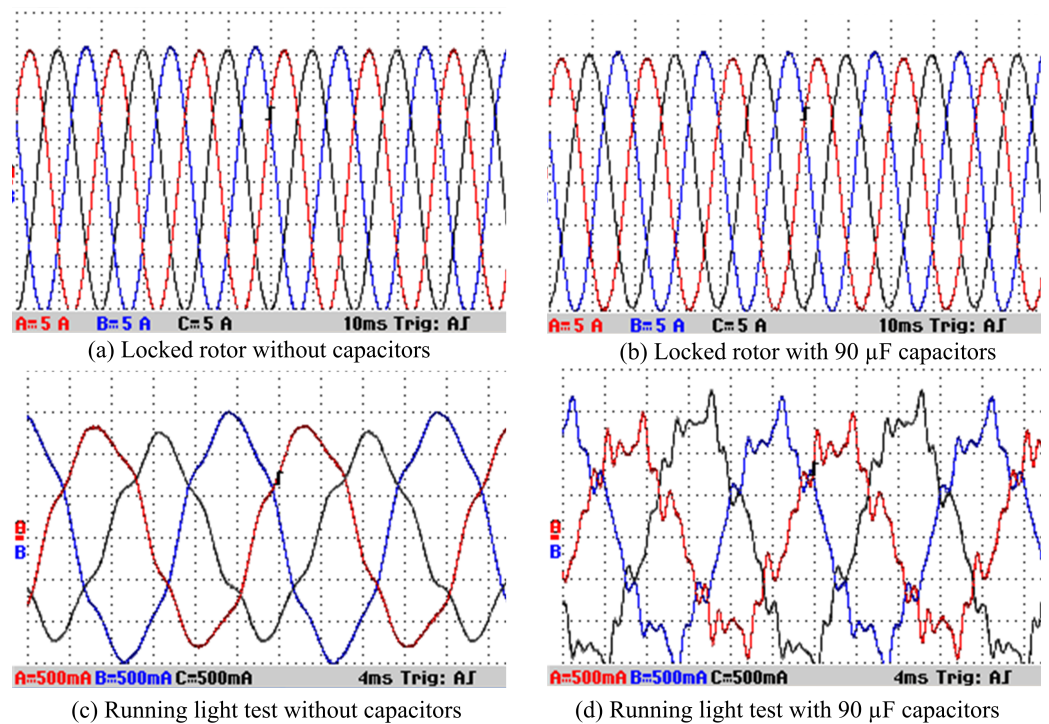


Figure 28. Current waveforms for Motor No. 1 at 100 V—currents with and without and 90 μF —for locked-rotor testing, the motor current was high and this is a resistive motor circuit so the capacitor currents were not noticeable, but for running light, the current was much reduced and the motor was more inductive so that the capacitor current was now visible.

6.2. Motor No. 1E Steady-State Testing—Running Light and Locked Rotor Tests

The running light and locked rotor tests were repeated with the same capacitor combinations using 50 μF and 90 μF capacitors. Tables 8 and 9 give the locked rotor tests and Tables 10 and 11 give the running light tests. Figure 24 shows the steady state simulation at a line voltage of 122.5 V rms with 90 μF capacitors. The locked rotor tests were conducted at a line voltage of 100 V rms, but the running light test requires the voltage to be increased to 109 V, to reach steady-state. The results in Figure 24 can be rationed to get the line currents with and without capacitors. The results appeared good in terms of correlation between the simulations and measurements; however, the measured currents with the capacitors seemed higher. Thus, it is worth looking at the locked-rotor current waveform. This is given in Figure 29 for the locked rotor condition with 90 μF capacitors. It can be observed

that there was substantial harmonic content, bearing in mind that this had no inductor filter for the capacitors.

Table 8. Motor No. 1E locked rotor test with and without 50 μF compensation capacitors.

100 V Line 50 μF Caps.	I_a	I_b	I_c	$I_{meanrms}$	$I_{meanpeak}$	$I_{Simpeak}$
Motor	5.34	5.41	5.45	5.4	7.64	7.02
Capacitors and motor	2.9	2.9	2.9	2.9	4.10	

Table 9. Motor No. 1E locked rotor test with and without 90 μF compensation capacitors.

100 V Line 90 μF Caps.	I_a	I_b	I_c	$I_{meanrms}$	$I_{meanpeak}$	$I_{Simpeak}$
Motor	5.45	5.65	5.61	5.57	7.88	7.02
Capacitors and motor	2	2.2	2.2	2.13	3.02	2.04

Table 10. Motor No. 1E running light test with and without 50 μF parallel compensation capacitors.

109 V Line 50 μF Caps.	I_a	I_b	I_c	$I_{meanrms}$	$I_{meanpeak}$	$I_{Simpeak}$
Motor	0.98	1.12	0.83	0.98	1.38	1.6
Capacitors and motor	1.9	2	2.3	2.07	2.92	

Table 11. Motor No. 1E running light test with and without 90 μF parallel compensation capacitors.

109 V Line 90 μF Caps.	I_a	I_b	I_c	$I_{meanrms}$	$I_{meanpeak}$	$I_{Simpeak}$
Motor	0.89	0.98	0.89	0.92	1.30	1.60
Capacitors and motor	4.2	4.8		4.85 4.62	6.53	6.23

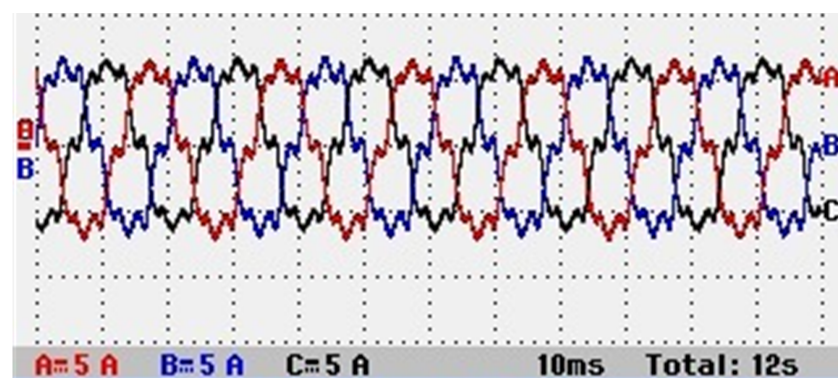


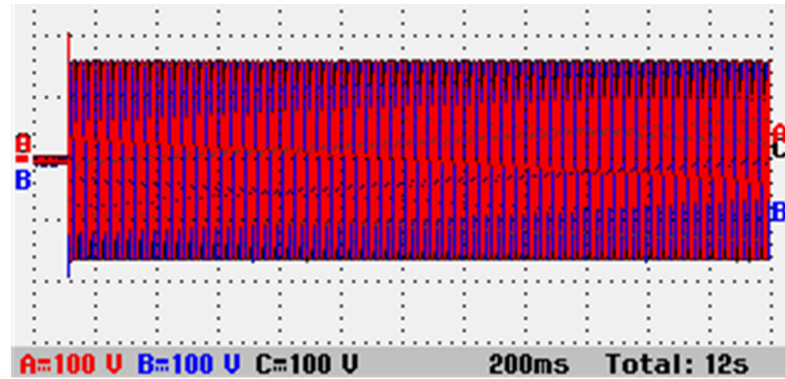
Figure 29. Locked-rotor current waveform for Motor No. 1E at 100 V—currents with 90 μF capacitors—there is now substantial harmonic in the locked-rotor current.

6.3. Motor No. 1E Transient Testing

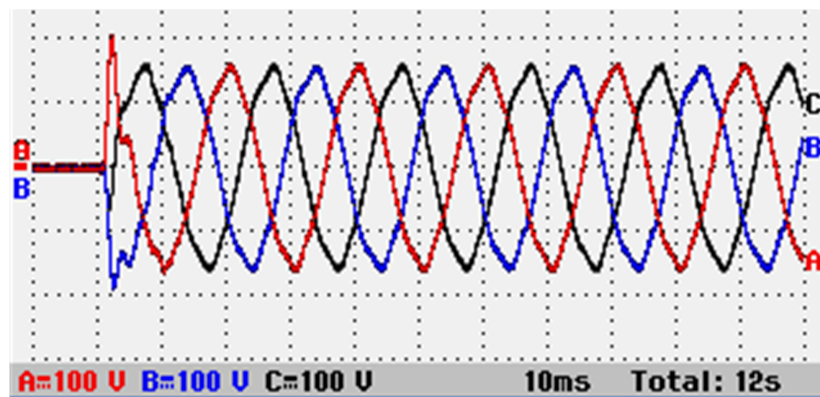
6.3.1. 1E with 90 μF Parallel Compensation Capacitors, Random 3-Phase Turn-on and No Capacitor Filtering

The system voltages are shown in Figure 30. The top graph showed constant voltage over the 2.2 s of the run-up. The second graphs shows a zoom to the start of the run-up. The switching is a random point and can be observed that there was some harmonic content. The data could be downloaded and a Fast Fourier Analysis conducted; however, here a

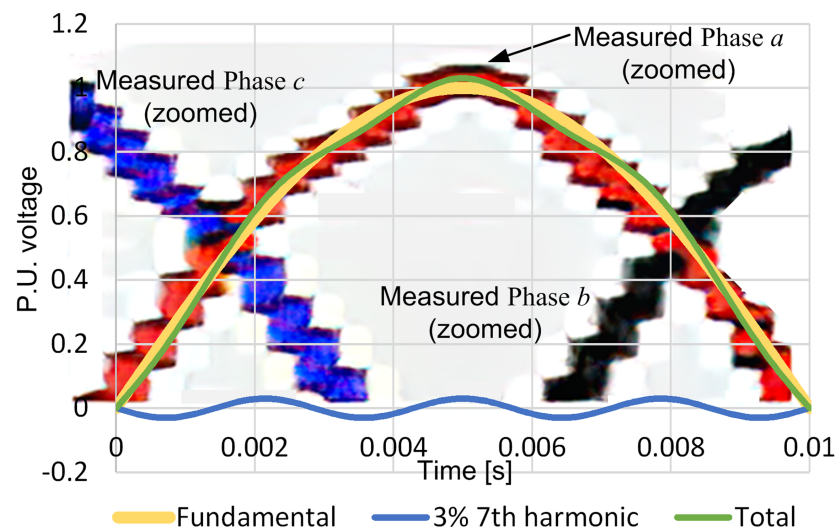
curve fit was created in Matlab with a sine wave and a 3% 7th harmonic and this fit the waveform well. This means that the harmonic current, with no filtering on the capacitors could be around $3 \times 7 = 21\%$ of the main capacitor current.



(a) start-up current; first 1.8 s.



(b) start-up current; first 110 ms.



(c) zoom of measured start-up current compared to current with 7th harmonic.

Figure 30. Transient system voltage waveforms for Motor No. 1E at 100 V—the voltage waveform in (c) shows about 3% of the 7th harmonic; (a,b) have 100V/div on the Y axis while (c) is in p.u.

For the 3% 7th harmonic, the harmonic voltage was $0.03 \times 170 = 5.1$ V peak for the line voltage. The capacitive harmonic reactance for a $90 \mu\text{F}$ capacitor was $1/(2\pi \times 350 \times 0.00009) = 5.05 \Omega$. The harmonic phase current in the delta-connected

capacitors was, therefore, $5.1/5.05 = 1.01$ A peak. This gives a peak harmonic line current $\sqrt{3} \times 1.01 = 1.74$ A so that the peak-to-peak harmonic current was 3.50 A. The main impedance was $1/(2\pi \times 50 \times 0.00009) = 35.37 \Omega$. This gave a peak line current of $\sqrt{3} \times 170/35.37 = 8.32$ A. This harmonic current would be a maximum. There will be supply inductance that may limit the current harmonics and the voltage may change with loading, i.e., the motor speed. It was found through the experiment that the size of the 7th order capacitor harmonic current was much lower than this even without a filter, and was heavily damped by the $j1.1 \Omega$ in-line inductor filters.

The transient turn-on current is shown in Figure 31 and this can be compared to Figure 25 for the transient envelope. This had an inertia of 0.12 kg m^2 and a friction torque of 0.625 Nm . The run-up time was about 5 s. The turn-on current spikes could be observed and these were quite high. Bearing in mind that this is random turn-on of all three phases and the capacitors had no filters.

A set of currents for the grid are shown in Figure 32. For repeatability, each current measurement was taken twice. The zoomed currents were shown at the start, illustrating the transient turn-on, at low speed, which showed harmonic current with about 3 A peak-to-peak, and the steady-state no-load current, which still had considerable harmonics and was trapezoidal in shape. These confirmed that there were current spikes during turn-on and that there was substantial harmonic current when there was no capacitor filter. The low-speed current waveforms showed harmonics close to that calculated above. The no-load grid current was higher than the low speed current because, at no-load, the grid current was dominated by the capacitor current, whereas at low speed, the induction motor and capacitor currents cancelled each other out—hence the dominant harmonic current.

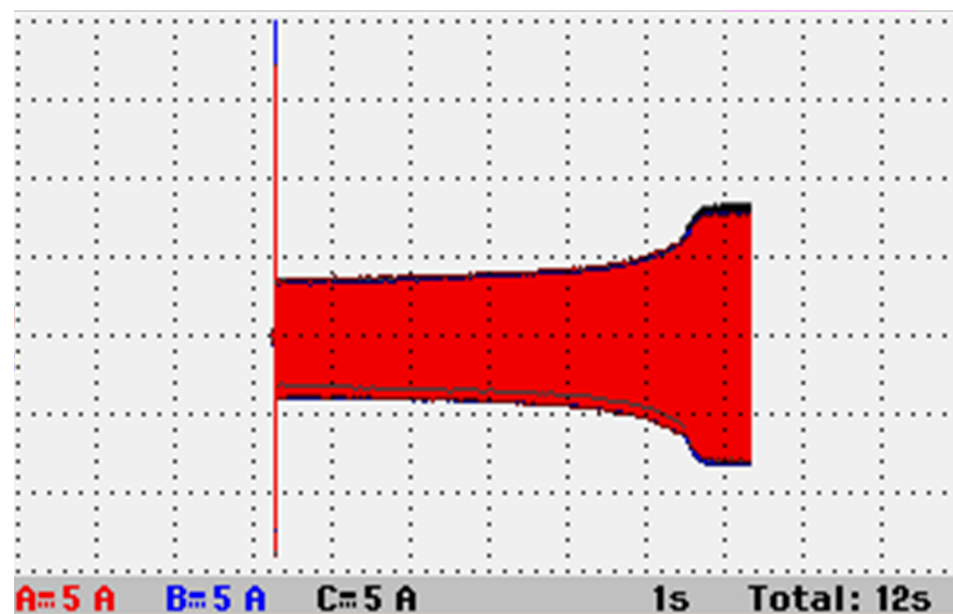


Figure 31. Transient system current for Motor No. 1E at 100 V peak for the phase—with $90 \mu\text{F}$ compensation capacitors in parallel. The X-axis is 1 s/div and Y-axis is 5 A/div. This shows the initial capacitor turn-on current spikes, then a period of the motor and capacitor currents cancelled, and the capacitor current dominated at no load (they should be switched out before this point was reached).

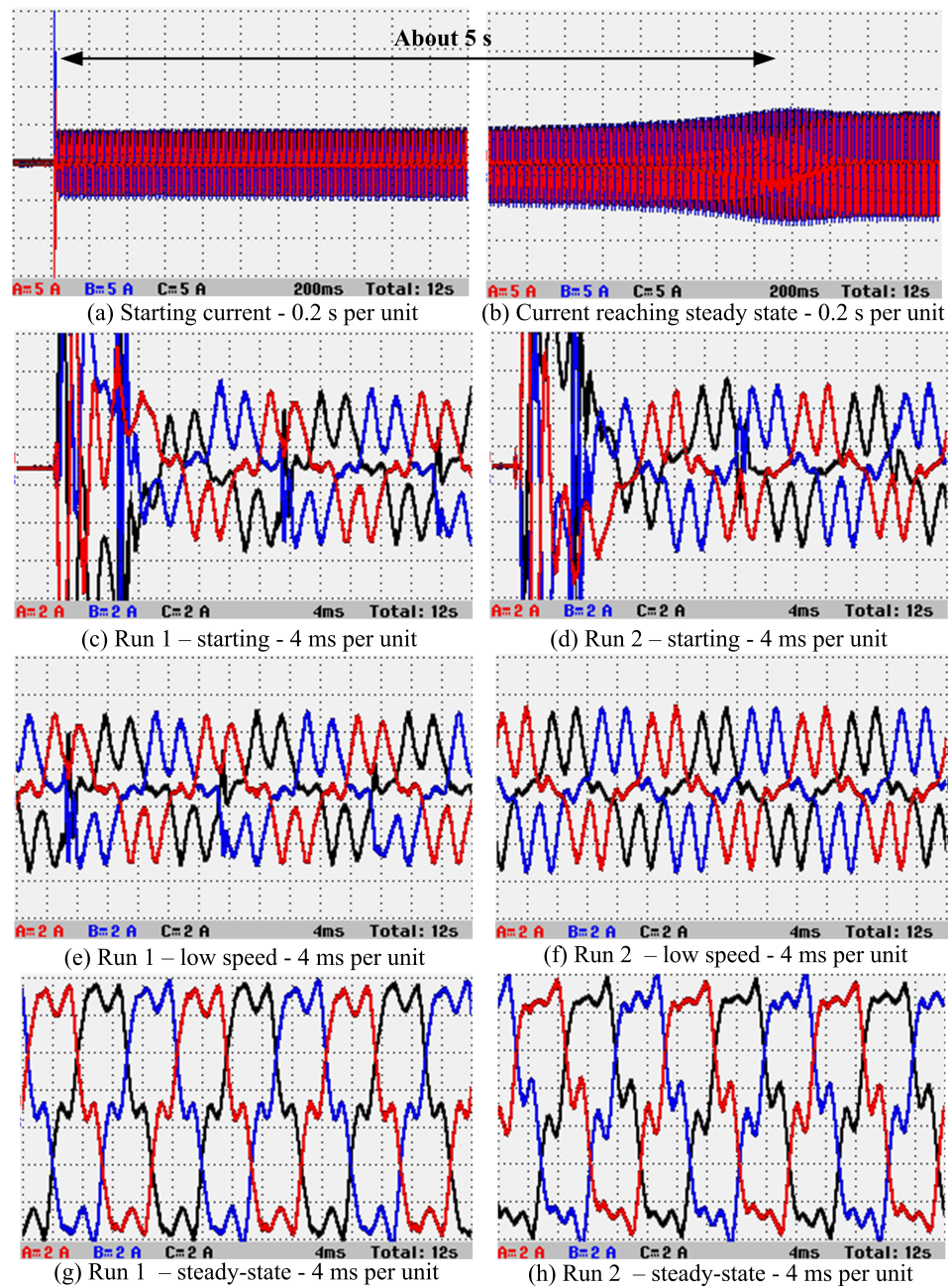


Figure 32. Transient system current for Motor No. 1E at 100 V phase peak—with 90 μ F parallel compensation capacitors, but with no capacitor filters. Y-scales: 5 A/division. A 7th harmonic would have a period of 2.86 ms, or 7 cycles every 20 ms—the waveforms all showed a harmonic of this order.

The motor currents are shown in Figure 33 across the range of speed as well as zooms at the start and in steady-state. Comparison with Figure 32 shows that the starting current was reduced considerably. The capacitors were not disconnected, so the steady-state grid current was higher than the motor current, as predicted. It can be seen in Figure 33 that there were no motor harmonics and the transient turn-on was only about 30% in the first cycle. Again, each waveform was recorded twice to show consistency.

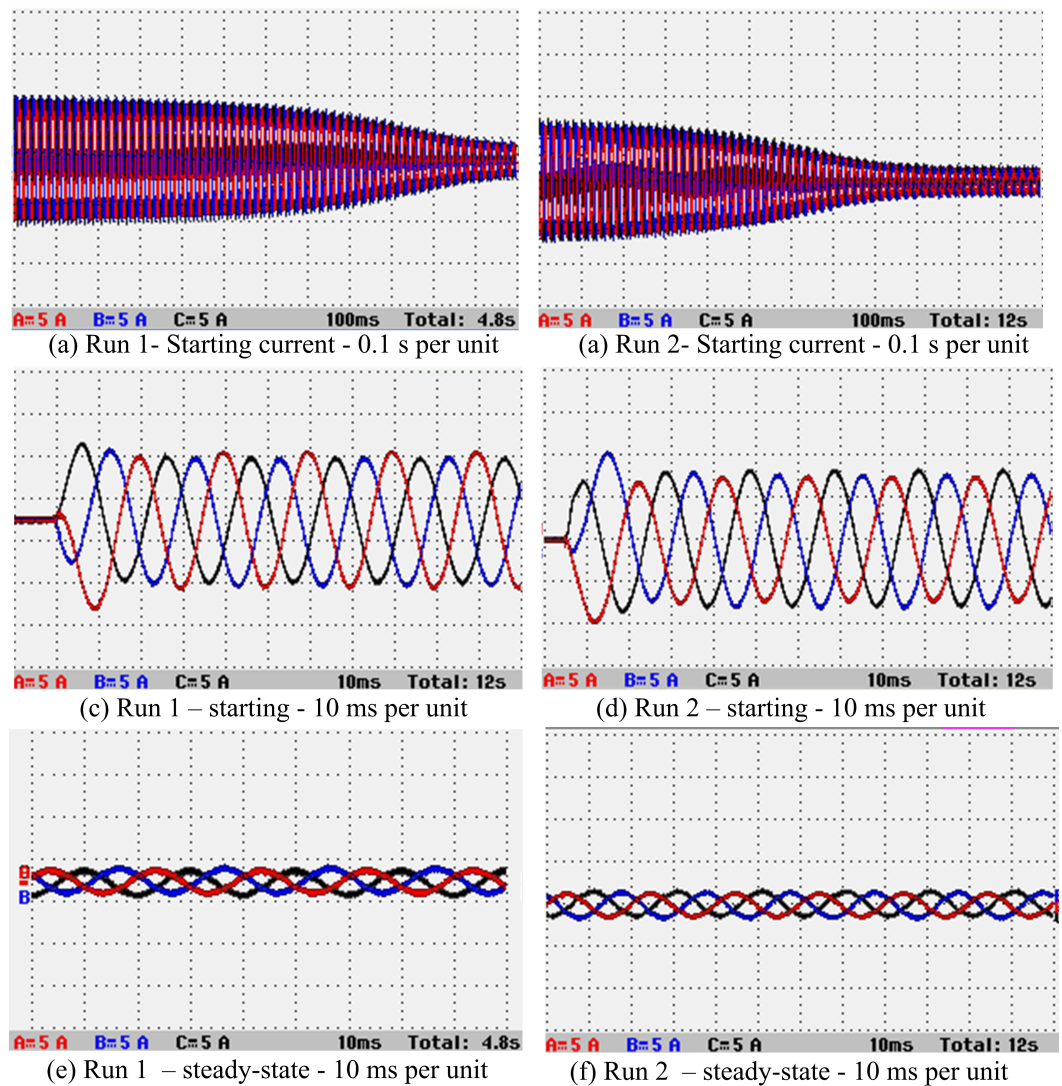


Figure 33. Transient motor current for Motor No. 1E at 100 V phase peak—with 90 μ F parallel compensation capacitors, but with no capacitor filters. Y-scales: 5 A/div. This illustrates that the harmonic currents in Figure 32 were not due to the motor.

Figure 34 shows the capacitor voltages and currents. The voltage had some spikes during turn-on and this was to be expected since the capacitor had no filter and was randomly switched across the grid. The currents are the difference between the grid and motor currents, and these contain current spikes during turn-on and distortion during operation due to harmonics.

The capacitor compensation method has been tested in the section on Motor No. 1E, and the capacitors have been shown to substantially reduce the run-up current by over 50%. However, filters appeared to be needed on the capacitors, which is investigated in the next section.

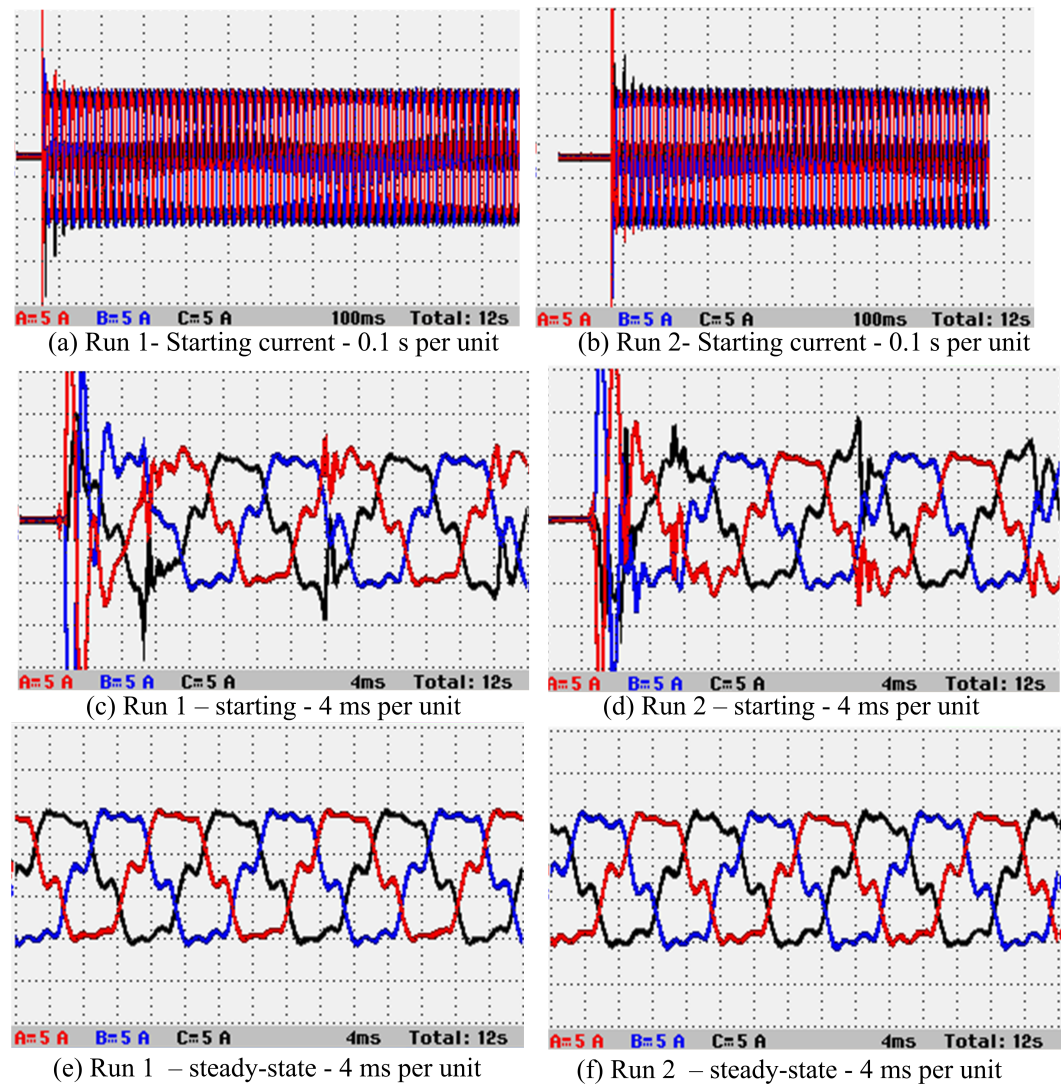


Figure 34. Transient capacitor current for Motor No. 1E at 100 V phase peak—with 90 μF parallel compensation capacitors, but with no capacitor filters. Y-scales: 5 A/div. It can be seen that the capacitor currents were almost trapezoidal and generating the harmonic currents in Figure 32. The total current in Figure 32 was the currents in this figure added to the currents in Figure 33.

6.3.2. 1E with 90 μF Parallel Compensation Capacitors, Random 3-Phase Turn-On but with Capacitor Filtering

Figure 35 shows the grid current when 1.1 Ω inductive filters were added in series with the 90 μF compensation capacitors. The waveforms showed the currents across parts of the run-up period, which was still about 5 s. Two different measurements were shown for each waveform. In (c) and (d), it can be seen that the turn-on transient current spikes were attenuated and less sharp. The low speed currents in (e) and (f) had less current harmonic when compared to Figure 32, illustrating the need for filtering. The steady-state currents in (g) and (h) are also not as trapezoidal and had less harmonics. In Figure 36, the capacitor currents were shown, again, showing a reduction in the current harmonic.

So far, the turn-on was through a normal breaker that has a random turn-on. To try to reduce the transient switch-on voltage and current spikes, then point-on switching was addressed in the next section.

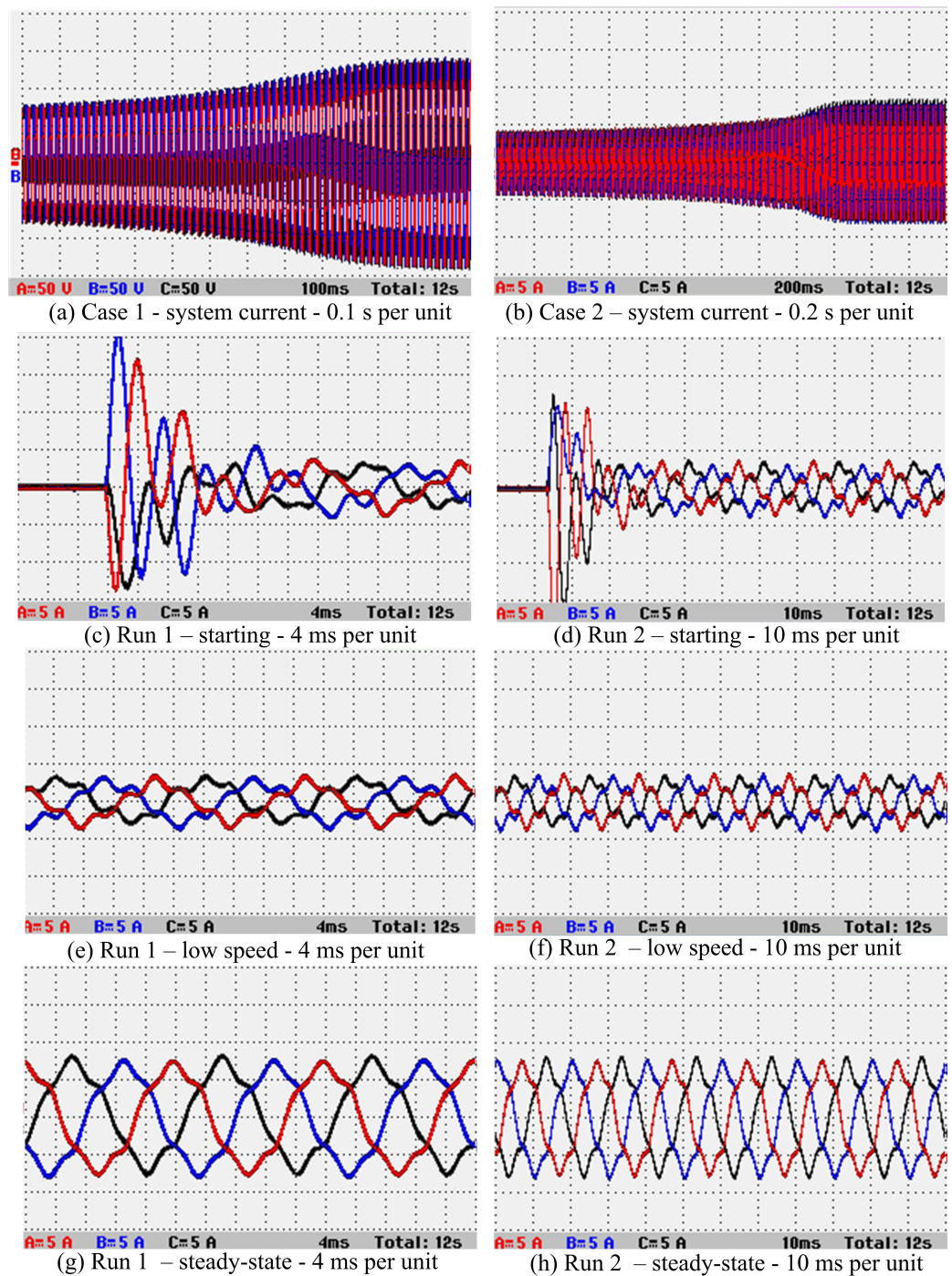


Figure 35. Transient system current for Motor No. 1E at 100 V phase peak—with 90 μ F capacitor and 1.1 Ω series inductor filter. Y-scales: top—5 A/unit, rest—2 A/unit. This clearly shows the filter reducing the grid current harmonic when compared to Figure 32.

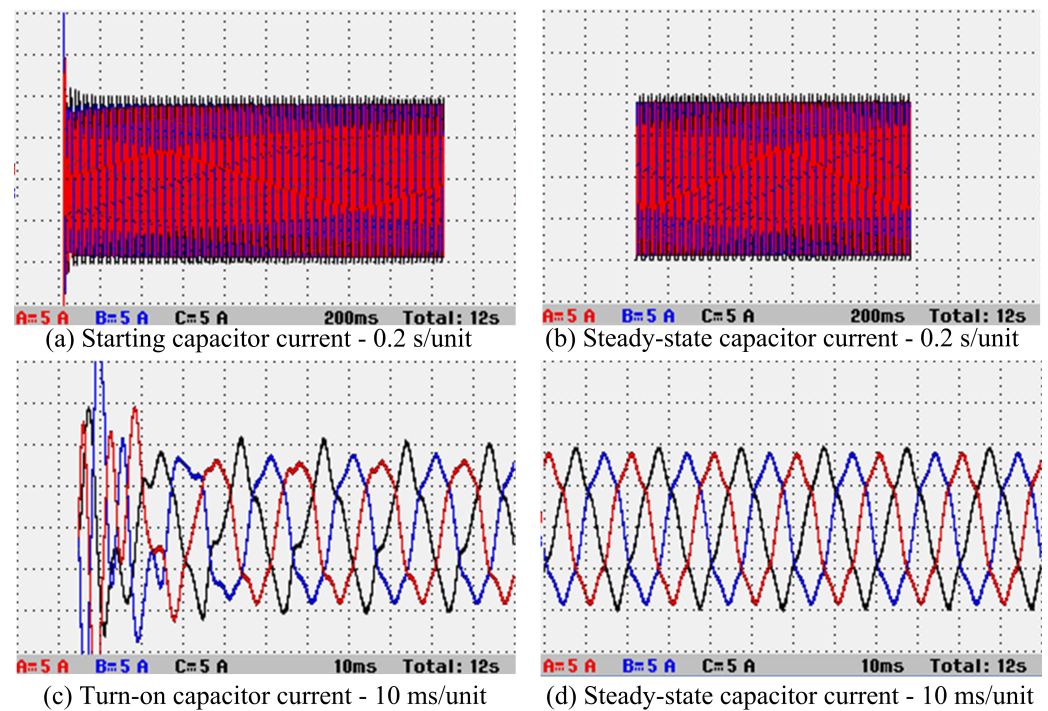


Figure 36. Transient capacitor current for Motor No. 1E at 100 V phase peak—with 90 μ F parallel compensation capacitors. Y-scales: top—5 A/unit, rest—2 A/unit. This shows a reduced harmonic content in the capacitor current when compared to Figure 34.

6.4. Point-On Switching

In this section, the effects of point-on switching were investigated. The system was built so that it could be switched on as the line voltage across Phases *a* and *b* through zero, then 90° later, when the voltage across the Phase *c* breaker was zero. Motor Nos. 1 and 1A were both tested here.

6.4.1. Motor No. 1 Switching

Motor No. 1 was tested first; hence, the machine had the series inductors removed and there was no capacitor compensation. Figure 37 shows the line voltages and currents during starting. It can be seen that the Phases *a* and *b* were connected first so that in (a) the blue line, and in (b) the black line, show a line voltage that starts at zero as the line voltage goes through the voltage crossing point and turn-on occurs. The other two line voltages were equal and half this since the star point was at the mid point between the two active phases. Then, 90° later, when Phase *c* was equal to star point, Phase *c* was switched on. The phasor diagram for illustrating this is shown in Figure 38.

Since this is a resistive motor at start, the overshoot was not high and this starting method did not offer much improvement over random switch-on. Bear in mind that at this stage, only the motor was switched on.

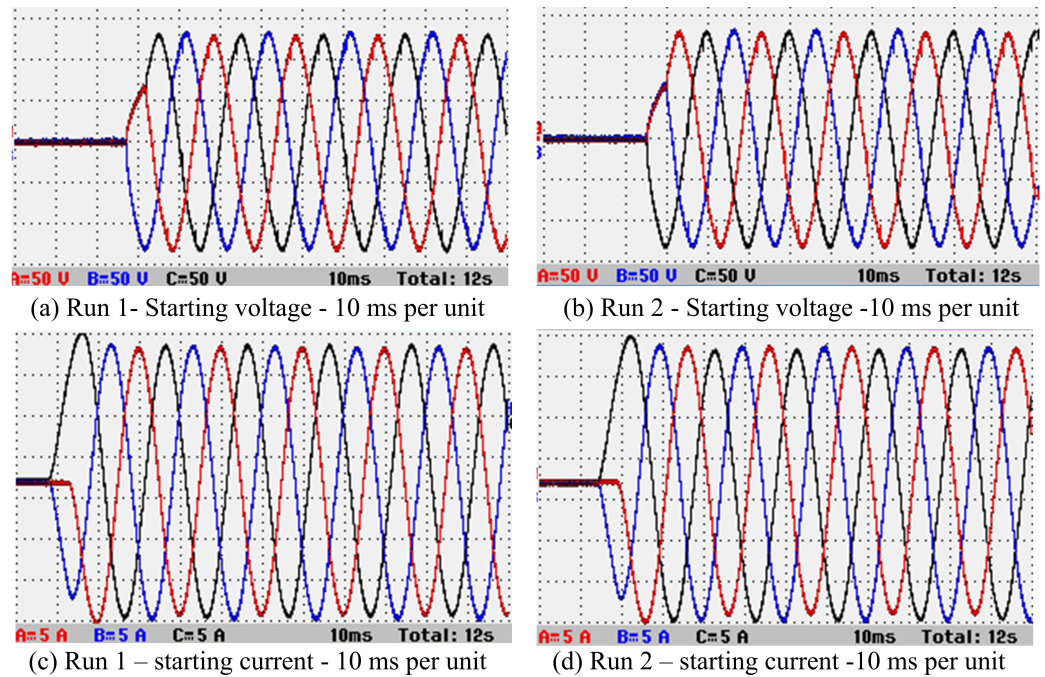


Figure 37. Turn-on line voltages and currents for Motor No. 1 at 100 V line rms. Y-scales: top—50 V/div, bottom—5 A/div.

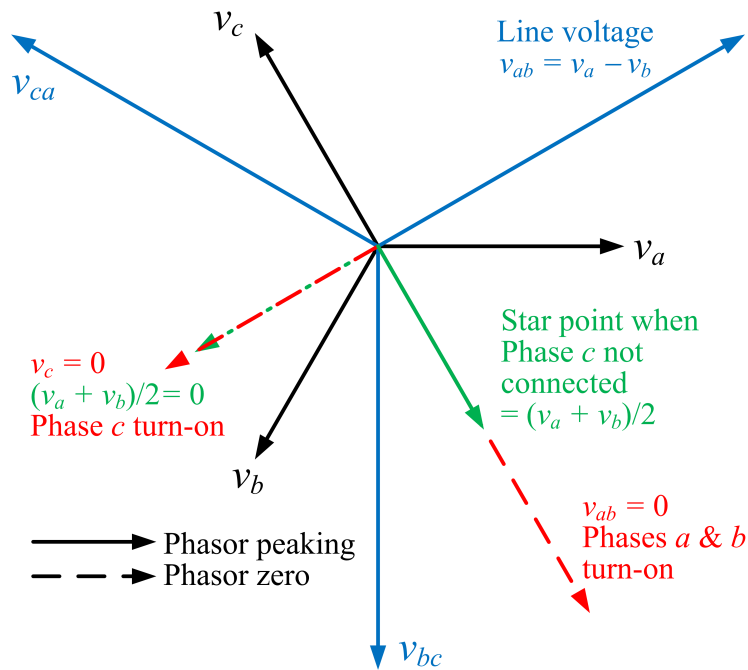


Figure 38. Phasor diagram for turn-on sequence.

6.4.2. Motor No. 1E Switching

For Motor No. 1E, the voltages and currents are shown in Figure 39. The switch-on occurred at the zero line current crossing points and it can be seen in (c) and (d) that the currents were opposite but with the same wave shape between Runs 1 and 2. The current was seen to have about 30% overshoot in the first cycle. However, when compared to Figure 33, there appeared to be little improvement in the transient motor turn-on current using the zero voltage crossing point method, even for this inductive motor. However, the switching method did give switch-gear protection.

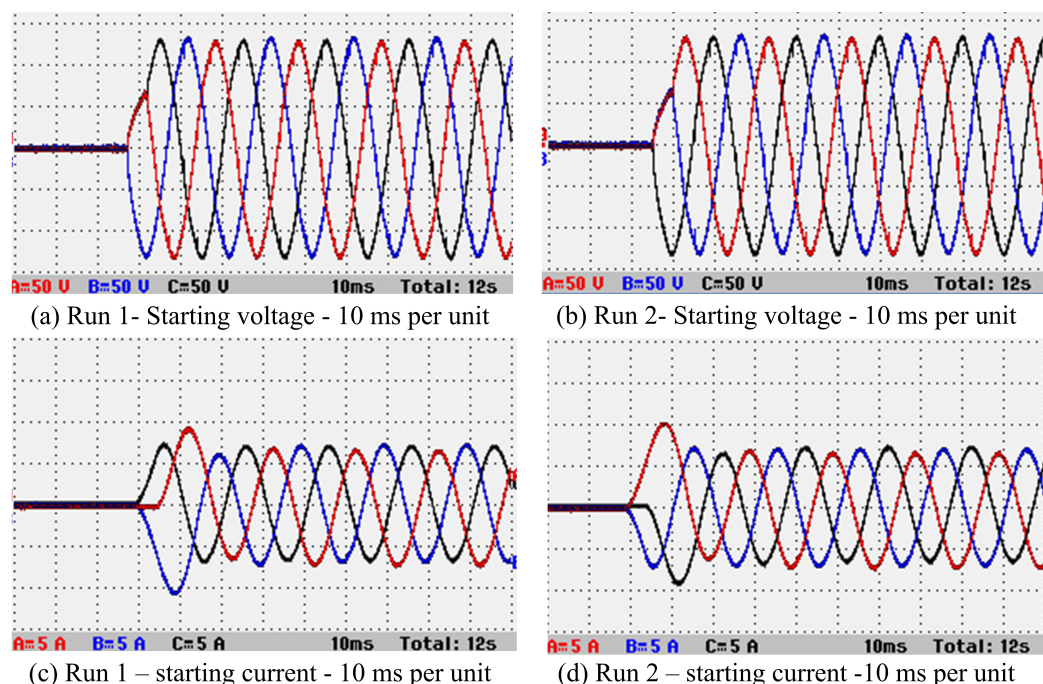


Figure 39. Turn-on line voltages and currents for Motor No. 1E at 100 V line rms. Y-scales: top—50 V/div, bottom—5 A/div.

6.4.3. Motor No. 1E Switching with Capacitors and Filters

The motor was switched on with the delta-connected capacitors connected in parallel. These had the 1.1Ω inductive filters in series. The measurements are given in Figure 40. It can be seen that the motor currents for Runs 1 and 2 in Figure 40c,d were the same and unaffected by the capacitors. There was still transient grid turn-on current. However, for random turn-on shown in Figure 32c,d the peak of the current spikes was 20 A. With the zero voltage cross point switching, as shown in Figure 40c,d, the grid turn-on current spikes appeared to be halved to about 10 A (the zoom in Figure 40e,f were zoomed to 2A/div so that spike peaks were not quite on the graph). This presents an improvement in the capacitor turn-on and the capacitors could be switched on with zero charge on the capacitor.

6.5. Discussion on Experimental Work

In the simulations, it was found that for larger induction motors there were more inductive and longer transient run-up times, so that the capacitor compensation method appeared to substantially reduce the starting current. First, a small induction motor that is more resistive was tested, as described in Section 6.1. The tables give measured values under locked rotor and running light conditions, with and without compensation capacitors, and the measured current values were found not to be reduced to the same extent compared to simulation. Figure 28 illustrated that the capacitors introduced harmonics into the grid current waveforms offsetting current reduction due to capacitor compensation.

It was shown that larger induction machines become more inductive in Figure 7 due to a slow increase in p.u. leakage reactance and a large decrease in p.u. resistance (which would also cause an increase in p.u. starting current), so inductance was added to the small motor so that it became more inductive. The grid supply had about 3% 7th voltage harmonic, as shown in Figure 30, which generates capacitor current harmonics. Therefore, filter inductors were added in series with the compensation capacitors. Figures 32–34 show the grid current, motor current and capacitor currents when no compensation capacitors were used and it can be clearly seen that there were no harmonics in the motor currents and that the capacitors were the source of the harmonics in the grid current. These can be compared to the results when the compensation capacitor filters were fitted, as

shown in Figure 35 for the total grid current drawn from the supply and Figure 36 for the capacitor current.

There was a substantial starting current reduction. Overall, there was about a 50% reduction in starting current when comparing the motor current in Figure 33, which showed 15 A peak-to-peak, with the system currents in Figure 35, which are about 7.5 A peak-to-peak.

The use of soft starting using point-on switching to reduce the turn-on current spikes was also demonstrated experimentally and this can be illustrated by comparison of Figure 36, which has spikes of well over 20 A peak with Figure 40, where point-on zero voltage-crossing switching is used, and the spikes were now about 10 A peak.

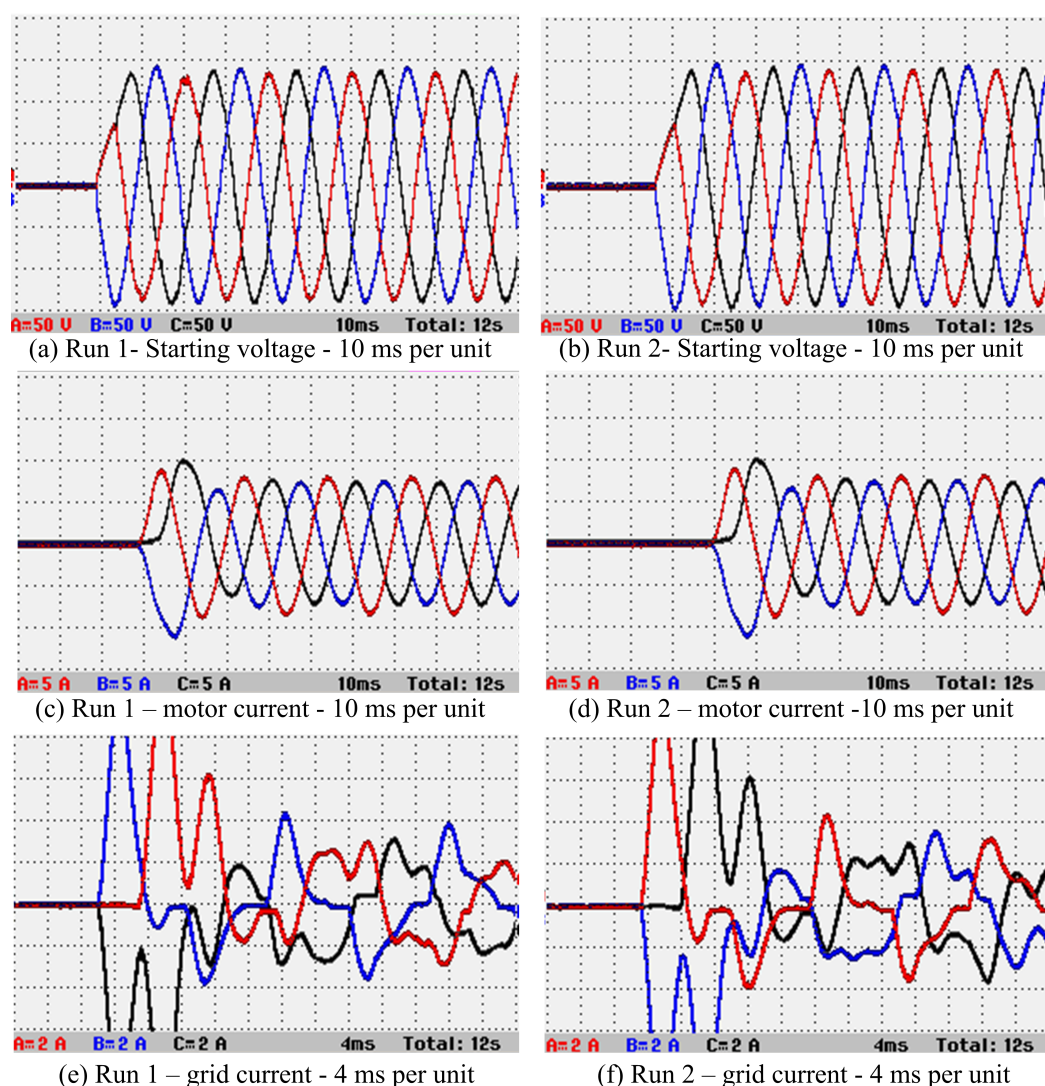


Figure 40. Turn-on line voltages and currents for Motor No. 1 at 100 V line rms. Y-scales: top—50 V/div, middle—5 A/div and bottom—2 A/div.

7. Conclusions

This paper has reported on simulation and experimental work carried out to show that the use of parallel capacitor compensation during turn on and run-up is effective in reducing the transient current in large induction motors. This method has not been fully reported before and a short survey on commercial motors shows that the method becomes more effective as the motor size increases. The work also investigated point-on switching to reduce turn-on (rather than run-up) current. It has been shown that for a large inductive-start motor there is considerable reduction in the start current when using

compensation capacitors. However, there needs to be filtering of the capacitors to reduce harmonics. It was shown that using in-line inductors with the capacitors reduced the run-up current harmonic considerably. This verified the simulations work.

The use of point-on switching was shown to be possible to reduce turn-on transients. This can be used to soft-start the motor and allow connection of the uncharged capacitors when the line voltage is zero. This appears to reduce the capacitor turn-on current spikes. The advantage of this method is to soft-connect equipment.

Further work will address the possible commercialization of the system with full capacitor turn-on and turn-off capabilities. Currently, this is an issue in many applications and there is no easy way to avoid high transient starting currents in large line-connected induction motors.

Author Contributions: Conceptualization, D.G.D.; methodology, D.G.D.; software, D.G.D. and M.H.; validation, M.H. and R.M.; formal analysis, D.G.D. and M.H.; investigation, D.G.D., M.H. and R.M.; resources, D.G.D.; data curation, D.G.D. and M.H.; writing—original draft preparation, D.G.D. and M.H.; writing—review and editing, D.G.D.; visualization, D.G.D.; supervision, D.G.D.; project administration, D.G.D.; funding acquisition, D.G.D. All authors have read and agreed to the published version of the manuscript.

Funding: The APC was funded by NRF BRICS Grant No. 116023.

Informed Consent Statement: Not applicable.

Data Availability Statement: Not applicable.

Conflicts of Interest: The authors declare no conflict of interest.

References

- Smith, T.P. Performing detailed power system studies for designing and analyzing electrical distribution systems—Power system studies for cement plants. *IEEE Ind. Appl. Mag.* **2007**, *13*, 56–65. [\[CrossRef\]](#)
- Saathoff, E.K.; Green, D.H.; Agustin, R.A.; O’Connell, J.; Leeb, S.B. Inrush Current Measurement for Transient Space Characterization and Fault Detection. *IEEE Trans. Instrum. Meas.* **2021**, *70*, 3520410. [\[CrossRef\]](#)
- Chapman, S. *Electric Machinery Fundamentals*; Tata McGraw-Hill Education: New York, NY, USA, 2005.
- Fuchs, E.; Masoum, M.A.S. *Power Quality in Power Systems and Electrical Machines*; Academic Press: Cambridge, MA, USA, 2011.
- Umans, S.D. Steady-state, lumped-parameter model for capacitor-run, single-phase induction motors. *IEEE Trans. Ind. Appl.* **1996**, *32*, 169–179. [\[CrossRef\]](#)
- Leng, S.; Ul Haque, R.; Perera, N.; Knight, A.M.; Salmon, J. Soft Start of Induction Motors using Floating Capacitor H-bridge Converters. In Proceedings of the 7th IET International Conference on Power Electronics, Machines and Drives (PEMD), Manchester, UK, 8–10 April 2014; pp. 1–6.
- Leng, S.; Ul Haque, R.; Perera, N.; Knight, A.M.; Salmon, J. Soft Start and Voltage Control of Induction Motors Using Floating Capacitor H-Bridge Converters. *IEEE Trans. Ind. Appl.* **2016**, *54*, 3115–3123. [\[CrossRef\]](#)
- Devadason, J.; Moses, P.S. Analysis of Free Acceleration and Steady State Characteristics of Line-Started Induction Motors with Shunt Capacitor Compensation. In Proceedings of the IEEE Power and Energy Society General Meeting (PESGM), Atlanta, GA, USA, 4–8 August 2019; pp. 1–5.
- Sen, P.K. Burlison, Induction motor overvoltage due to power factor improvement capacitor. In Proceedings of the Conference Record of the IEEE Industry Applications Society Annual Meeting, San Diego, CA, USA, 1–5 October 1989.
- Locke, C. Optimal capacitor sizing for induction motors. In Proceedings of the Conference Canadian Conference on Electrical and Computer Engineering, Halifax, NS, Canada, 7–10 May 2000.
- Kolar, J.W.; Biela, J.; Waffler, S.; Friedli, T.; Badstuebner, U. Performance trends and limitations of power electronic systems. In Proceedings of the 6th International Conference on Integrated Power Electronics Systems, Nuremberg, Germany, 14–16 March 2010; pp. 1–20.
- Ferreira, F.J.T.E.; Fong, J.A.C.; de Almeida, A.T. Ecoanalysis of Variable-Speed Drives for Flow Regulation in Pumping Systems. *IEEE Trans. Ind. Electron.* **2011**, *58*, 2117–2125. [\[CrossRef\]](#)
- Rehaoulia H.; Poloujadoff, M. Transient behavior of the resultant airgap field during run-up of an induction motor. *IEEE Trans. Energy Convers.* **1986**, *EC-1*, 92–98. [\[CrossRef\]](#)
- Banach, H. Condition for the Occurrence of Maximum Efficiency in Induction Motors and Transformers. In Proceedings of the International Symposium on Electrical Machines (SME), Andrychow, Poland, 10–13 June 2018; pp. 1–5.
- Itajiba, J.A.; Varnier, C.A.C. Cabral, S.H.L.; Stefenon, S.F.; Leithardt, V.R.Q.; Ovejero, R.G.; Nied, A.; Yow, K.-C. Experimental Comparison of Preferential vs. Common Delta Connections for the Star-Delta Starting of Induction Motors. *Energies* **2021**, *14*, 1318. [\[CrossRef\]](#)

16. Saifulin, R.; Pajchrowski, T.; Breido, I. A Buffer Power Source Based on a Supercapacitor for Starting an Induction Motor under Load. *Energies* **2021**, *14*, 4769. [[CrossRef](#)]
17. Singh, B.; Adya, A.; Mittal, A.P.; Gupta, J.R.P.; Singh, B.N. Application of DSTATCOM for Mitigation of Voltage Sag for Motor Loads in Isolated Distribution Systems. In Proceedings of the IEEE International Symposium on Industrial Electronics, Montreal, QC, Canada, 9–13 July 2006.
18. McElveen, R.F.; Toney, M.K. Starting high-inertia loads. *IEEE Trans. Ind. Appl.* **2001**, *37*, 137–144. [[CrossRef](#)]
19. Biot-Monterde, V.; Navarro-Navarro, A.; Antonino-Daviu, J.A.; Razik, H. Stray Flux Analysis for the Detection and Severity Categorization of Rotor Failures in Induction Machines Driven by Soft-Starters. *Energies* **2021**, *14*, 5757. [[CrossRef](#)]
20. Kurtz, E.B. Transformer current and power inrushes under load. *Electr. Eng.* **1937**, *56*, 989–994. [[CrossRef](#)]
21. Hayward, C.D. Prolonged inrush currents with parallel transformers affect differential relaying. *Electr. Eng.* **1941**, *60*, 1096–1101. [[CrossRef](#)]
22. Akherraz, M. Inrush current and speed regulation of induction motor drives. In Proceedings of the 6th Mediterranean Electrotechnical Conference, Ljubljana, Slovenia, 22–24 May 1991; pp. 1285–1288.
23. Kron, G. *Equivalent Circuits of Electrical Machinery*; Wiley & Sons: New York, NY, USA, 1951.
24. Alger, P.L. *Induction Machines—Their Behavior and Uses*, 1st ed.; Gordon and Breach: New York, NY, USA, 1965.
25. Torrent, M.; Blanqué, B. Influence of Equivalent Circuit Resistances on Operating Parameters on Three-Phase Induction Motors with Powers up to 50 kW. *Energies* **2021**, *14*, 7130. [[CrossRef](#)]
26. Dorrell, D.G.; Holik, P.J.; Lombard, P.; Thougard, H.-J.; Jensen, F. Multisliced Finite-Element Model for Induction Machines Incorporating Interbar Current. *IEEE Trans. Ind. Appl.* **2009**, *45*, 131–141. [[CrossRef](#)]
27. Dorrell, D.G.; Holik, P.J.; Rasmussen, C.B. Analysis and Effects of Inter-bar Current on a Long Skewed-rotor Induction Motor for Pump Applications. *IEEE Trans. Magn.* **2007**, *43*, 2534–2536. [[CrossRef](#)]
28. Jabr, H.B.; Kar, N.C. Starting Performance of Saturated Induction Motors. In Proceedings of the IEEE Power Engineering Society General Meeting, Tampa, FL, USA, 24–28 June 2007.
29. Molsa, E.; Saarakkala, S.E.; Hinkkanen, M.; Arkkio, A.; Routimo, M. A Dynamic Model for Saturated Induction Machines With Closed Rotor Slots and Deep Bars. *IEEE Trans. Energy Convers.* **2020**, *35*, 157–165. [[CrossRef](#)]
30. Ikeda, M.; Hiyama, T. Simulation Studies of the Transients of Squirrel-Cage Induction Motors. *IEEE Trans. Energy Convers.* **2007**, *22*, 233–239. [[CrossRef](#)]
31. Erdogan, N.; Henao, H.; Grisel, R. The analysis of saturation effects on transient behavior of induction machine direct starting. In Proceedings of the IEEE International Symposium on Industrial Electronics, Ajaccio, France, 4–7 May 2004; Volume 2, pp. 975–979.
32. Meng, F.; Wang, D.; Liu, Z.; Su, W. Fast Circuit-Field Coupling Analysis for Skewed Induction Motor. *IEEE Trans. Ind. Electron.* **2021**, *68*, 5088–5099. [[CrossRef](#)]
33. Kim, J.; Hong, J.; Nam, K. A current distortion compensation scheme for four-switch inverters. *IEEE Trans. Power Electron.* **2009**, *24*, 1032–1040.
34. Linders, J.R. Effects of power supply variations on AC motor characteristics. *IEEE Trans. Ind. Appl.* **1972**, *IA-8*, 383–400. [[CrossRef](#)]
35. Wagner, V.E.; Balda, J.C.; Griffith, D.C.; McEachern, A.; Barnes, T.M.; Hartmann, D.P.; Phileggi, D.J.; Emmanuel, A.E.; Horton, W.F.; Reid, W.E.; et al. Effects of harmonics on equipment. *IEEE Trans. Power Deliv.* **1993**, *8*, 672–680. [[CrossRef](#)]
36. Barnes, R. Harmonics in power systems. *IEE Power Eng. J.* **1989**, *3*, 11–15. [[CrossRef](#)]
37. Dudley, R.; Castanheira, A.; Sharp, M. Section 3.7: Reactors. *The Electric Power Engineering Handbook*, 3rd ed.; Grigsby, L.L., Ed.; CRC Press: Boca Raton, FL, USA, 2018; pp. 3–95.
38. Olivier, G.; Mougharbel, I.; Dobson-Mack, G. Minimal transient switching of capacitors. *IEEE Trans. Power Deliv.* **1993**, *8*, 1988–1994. [[CrossRef](#)]
39. Rahim, Y.H.A. Excitation of isolated three-phase induction generator by a single capacitor. *IEE Proc. B Electr. Power Appl.* **1993**, *140*, 44–50. [[CrossRef](#)]
40. How to Read a Positive Displacement Pump Curve. Available online: <https://www.csidesigns.com/blog/articles/how-to-read-a-positive-displacement-pump-curve> (accessed on 17 December 2021).
41. Mutize, C.; Wang, R.-J. Performance comparison of an induction machine and line-start PM motor for cooling fan applications. In Proceedings of the 21st Southern African Universities Power Engineering Conference (SAUPEC), Potchefstroom, South Africa, 31 January–1 February 2013; pp. 122–126.
42. Valiadis Hellenic Motors. Available online: <https://www.valiadis.gr/> (accessed on 17 December 2021).
43. Sun, P.C. *Principles of Electric Machines and Power Electronics*; Wiley: Hoboken, NJ, USA, 1989.